Cellular/Molecular

Ca^{2+}/cAMP-Sensitive Covariation of I_A and I_H Voltage Dependences Tunes Rebound Firing in Dopaminergic Neurons

Julien Amendola,[1,2]* Adele Woodhouse,[1,2,3]* Marie-France Martin-Eauclaire,[2,4] and Jean-Marc Goaillard[1,2]

[1]Institut National de la Santé et de la Recherche Médicale UMR1072, Marseille 13015, France, [2]Aix Marseille Université, Faculté de Médecine Secteur Nord, Marseille 13015, France, [3]Menzies Research Institute Tasmania, University of Tasmania, Hobart, Tasmania 7000, Australia, and [4]Centre de Recherche Neurobiologie-Neurophysiologie de Marseille, Centre National de la Recherche Scientifique, Marseille 13015, France

The level of expression of ion channels has been demonstrated to vary over a threefold to fourfold range from neuron to neuron, although the expression of distinct channels may be strongly correlated in the same neurons. We demonstrate that variability and covariation also apply to the biophysical properties of ion channels. We show that, in rat substantia nigra pars compacta dopaminergic neurons, the voltage dependences of the A-type (I_A) and H-type (I_H) currents exhibit a high degree of cell-to-cell variability, although they are strongly correlated in these cells. Our data also demonstrate that this cell-to-cell covariability of voltage dependences is sensitive to cytosolic cAMP and calcium levels. Finally, using dynamic clamp, we demonstrate that covarying I_A and I_H voltage dependences increases the dynamic range of rebound firing while covarying their amplitudes has a homeostatic effect on rebound firing. We propose that the covariation of voltage dependences of ion channels represents a flexible and energy-efficient way of tuning firing in neurons.

Introduction

The ability of any specific ion channel to participate in a given firing feature (e.g., spike duration, spike amplitude, burst duration, rebound properties) has been studied and described in many different neuronal types in numerous invertebrate and vertebrate species (Hille, 2001). More recently, experimental and theoretical studies have suggested that whenever multiple currents contribute to the same firing feature, numerous solutions are available to cells to achieve the same output (Goldman et al., 2001; MacLean et al., 2003; Prinz et al., 2004; Burdakov, 2005; Swensen and Bean, 2005; Marder and Goaillard, 2006; Schulz et al., 2006; Puopolo et al., 2007; Taylor et al., 2009; Hudson and Prinz, 2010; Marder and Taylor, 2011). In mouse cerebellar Purkinje cells, knocking down the $Na_v1.6$ sodium channel does not significantly disrupt bursting behavior because the effect of knocking down this channel is partially compensated by an increase in amplitude of a low-threshold calcium current (Swensen and Bean, 2005). In the lobster stomatogastric nervous system, microinjecting pacemaker neurons with mRNA encoding for the *Shal* channel [carrying the rapidly inactivating A-type (I_A) potassium current] does not modify spontaneous bursting because the increase in I_A is compensated by a correlated increase in the amplitude of the hyperpolarization-activated H-type (I_H) cationic current (MacLean et al., 2003).

These studies using artificial manipulations of ion channel expression have led to the hypothesis that coregulation of properties of functionally overlapping ion channels in unperturbed neurons may constitute a powerful mechanism for precisely defining specific firing patterns and maintaining them over the lifetime of a neuron (Marder and Goaillard, 2006). Consistent with this hypothesis, recent studies performed in the invertebrate nervous system have demonstrated that numerous ion channels/currents display correlated levels of expression/amplitude in unperturbed populations of neurons (MacLean et al., 2005; Schulz et al., 2006, 2007; Khorkova and Golowasch, 2007; Goaillard et al., 2009; Tobin et al., 2009; Temporal et al., 2011). Moreover, some of these correlations in ion channel properties were demonstrated to be cell-type specific and strongly predict the functional output of the neuron (Schulz et al., 2007; Goaillard et al., 2009). Yet little is known about whether coregulation of ion channels occurs in unperturbed mammalian neurons, and whether they involve biophysical properties and/or the level of expression/amplitude of channels/currents.

We studied rebound firing in substantia nigra pars compacta (SNc) dopaminergic neurons and analyzed the respective involvement of I_H and I_A in this firing feature. First, we demonstrate that these two currents have opposite and complementary influences on rebound delay. We show that the voltage dependences of I_H and I_A are highly variable from cell to cell but are strongly positively correlated in the same cells. We then demonstrate that intracellular cAMP and calcium levels strongly alter the covaria-

Received Oct. 20, 2011; revised Nov. 28, 2011; accepted Dec. 12, 2011.

Author contributions: J.-M.G. designed research; J.A., A.W., M.-F.M.-E., and J.-M.G. performed research; J.A., A.W., and J.-M.G. analyzed data; J.A., A.W., and J.-M.G. wrote the paper.

This work was funded by Institut National de la Santé et de la Recherche Médicale (Avenir Grant to J.-M.G., postdoctoral fellowship to J.A.), the Fyssen Foundation (J.-M.G.), Conseil Général des Bouches du Rhône CG13 (J.-M.G.), the National Health and Medical Research Council of Australia (postdoctoral overseas training fellowship 544940 to A.W.) and the Foundation pour la Recherche Médicale (postdoctoral fellowship to A.W.). We thank Armand Tasmadjian and Martial Dufour for technical assistance; Dr. Hélène Vacher, Dr. Fabien Tell, and Dr. Dominique Debanne for helpful discussions on the experiments; and Dr. Dominique Debanne, Dr. Michael Seagar, and Dr. Eve Marder for helpful comments on the manuscript.

*J.A. and A.W. contributed equally to this work.

The authors declare no competing financial interest.

Correspondence should be addressed to Jean-Marc Goaillard, Avenir group Homeostasis of Excitability and Neuromodulation, Institute National de la Santé et de la Recherche Médicale UMR1072, Marseille 13015, France. E-mail: jean-marc.goaillard@univ-amu.fr.

DOI:10.1523/JNEUROSCI.5297-11.2012

 0270-6474/12/322166-16$15.00/0

tion of I_A and I_H voltage dependences. Strikingly, increasing cAMP in the presence of a fast calcium chelator induces a coordinated shift in the voltage dependences and reduces their variability. Finally, we show that covarying the maximum conductances of these currents stabilizes rebound firing, while covarying the voltage dependences of the currents according to their biological distribution increases the dynamic range of rebound firing. We suggest that covariation of voltage dependences provides a flexible and efficient way of tuning rebound firing.

Materials and Methods

Midbrain slice preparation. Acute slices were prepared from P16–P22 Wistar rats of either sex. All experiments were performed according to the European and institutional guidelines for the care and use of laboratory animals (Council Directive 86/609/EEC and French National Research Council). Rats were anesthetized with halothane (Nicholas Piramal India) and decapitated. The brain was immersed briefly in oxygenated ice-cold low-calcium artificial CSF (aCSF) containing the following (in mM): 125 NaCl, 25 $NaHCO_3$, 2.5 KCl, 1.25 NaH_2PO_4, 0.5 $CaCl_2$, 4 $MgCl_2$, and 25 glucose, pH 7.4, oxygenated with 95% O_2/5% CO_2 gas. The cortices were removed and then coronal midbrain slices (250 μm) were cut in ice-cold oxygenated low-calcium aCSF on a vibratome (Leica VT 1200S). Following 30–45 min incubation in oxygenated low-calcium aCSF at 32°C, the acute slices were then incubated for a minimum of 30 min in oxygenated aCSF (containing in mM: 125 NaCl, 25 $NaHCO_3$, 2.5 KCl, 1.25 NaH_2PO_4, 2 $CaCl_2$, 2 $MgCl_2$, and 25 glucose, pH 7.4, oxygenated with 95% O_2/5% CO_2 gas) at room temperature before electrophysiological recordings.

Drugs. We used kynurenate (2 mM, Sigma-Aldrich), picrotoxin (100 μM, Sigma-Aldrich), tetrodotoxin (TTX; 1 μM, Alomone Labs), ZD7288 (3 and 30 μM, Tocris Bioscience), *Androctonus mauretanicus mauretanicus* toxin 3 (AmmTX3, 3 nM–2 μM), 1,2-bis(2-aminophenoxy) ethane-*N*,*N*,*N*′,*N*′-tetra-acetic acid (BAPTA; 5 or 10 mM, Tocris Bioscience), 2′,5′-dideoxy adenosine 3′-triphosphate tetrasodium (ddA; 20 μM, Sigma-Aldrich), and 8-Bromo-cAMP sodium salt (8-Br-cAMP; 25 μM, Tocris Bioscience). Kynurenate, picrotoxin, tetrodotoxin, ZD7288, and AmmTX3 were used to block excitatory synaptic activity, inhibitory synaptic activity (current-clamp recordings), the TTX-sensitive sodium currents (voltage-clamp recordings), and the I_H and I_A currents, respectively, and were bath applied via continuous perfusion in aCSF, except for concentrations of AmmTX3 ≥30 nM (which were applied directly into the bath with the bath perfusion briefly arrested until the toxin took effect). BAPTA, ddA, and 8-Bromo-cAMP were present in the patch pipette solution.

Electrophysiology recordings and analysis. All recordings (342 cells in current-clamp, voltage-clamp, or dynamic clamp) were performed on midbrain slices continuously superfused with oxygenated aCSF at 30–32°C. Picrotoxin and kynurenate were systematically added to the aCSF for all recordings to prevent contamination of the intrinsically generated activity by glutamatergic and GABAergic spontaneous synaptic activity. Patch pipettes (1.8–2.5 MΩ for voltage-clamp recordings) were pulled from borosilicate glass (GC150TF-10 for voltage-clamp, Harvard Apparatus) on a DMZ-Universal Puller (Zeitz Instruments) and filled with a patch solution containing the following (in mM): 20 KCl, 10 HEPES, 10 EGTA, 2 MgCl2, 2 Na-ATP, and 120 K-gluconate, pH 7.4, 290–300 mOsm. Whole-cell recordings were made from SNc dopaminergic neurons visualized using infrared differential interference contrast videomicroscopy (QImaging Retiga camera; Olympus BX51WI microscope), and were identified based on their location, large size (soma >30 μm; see Fig. 1*A*), and electrophysiological profile (regular slow pacemaking activity, large spike half-width, large sag in response to hyperpolarizing current steps; see Fig. 1*C*,*D*). Tyrosine-hydroxylase immunolabeling in 73 neurobiotin (0.05% in patch solution; Vector Labs) tracer-filled cells confirmed this electrophysiological identification (see Fig. 1*B*). Briefly, slices were fixed with 4% paraformaldehyde overnight at 4°C and were immunolabeled (protocol modified from Wolfart et al., 2001) with sheep antityrosine hydroxylase (Millipore; 1:9000), followed by donkey anti-sheep Alexa Fluor 488 (Invitrogen; 1:1000; 2 μg/ml) and Streptavadin Alexa Fluor 594 (Invitrogen; 1:12,000; 166.7 ng/ml).

For voltage-clamp experiments, only whole-cell recordings with an uncompensated series resistance <7 MΩ (compensated 85–90%) were included in the analysis. For current-clamp pharmacology experiments, higher series resistances were tolerated as long as the bridge compensation was properly adjusted to 100%. Liquid junction potential (+13.2 mV) and capacitive currents were compensated on-line. To ensure that variability in voltage measurements was not due to the slow appearance of offset potentials during the recording, offset potentials were measured after removing the pipette from the neuron. Offset values were negligible (≤1 mV) and therefore not corrected for. Recordings were acquired at 10 kHz and were filtered with a low-pass filter (Bessel characteristic 2.9 kHz cutoff frequency). For current-clamp recordings, 1 s hyperpolarizing current steps were injected to elicit a hyperpolarization-induced sag (due to I_H activation). Short synaptic-like hyperpolarizing currents were also injected to mimic a single GABAergic input (diexponential inputs; 4.6 ms rising time constant, 47.4 ms decaying time constant) (Tanaka et al., 2009). For proper comparison of rebound properties across cells and pharmacological conditions, long hyperpolarizing current steps were adjusted to obtain an average voltage value of either −84.9 ± 1.8 mV or −71.9 ± 1.3 mV at the end of the hyperpolarizing pulse in all cells, and short synaptic-like hyperpolarizing inputs were adjusted to obtain an average voltage value of −84.9 ± 2.1 mV or −71.9 ± 1.5 mV at the peak of the hyperpolarization. V_{kink} was defined as the voltage point where the voltage first derivative reaches a plateau (corresponding to the start of the linear phase II).

For voltage-clamp recordings of I_A and I_H, tetrodotoxin was also added to the aCSF. The total potassium current was elicited by 500 ms voltage steps from a holding voltage of −100 mV to test potential between −80 and −5 mV (500 ms, 5 mV increments). The delayed rectifier potassium current was elicited by a protocol consisting of a 500 ms prestep at −50/−40 mV (to fully inactivate I_A) followed by voltage steps between −50/−40 and 10 mV (500 ms, 5 mV increments). The I_A current was then isolated by subtraction (total potassium current − delayed rectifier current). The peak of the isolate I_A measured during the incremental pulses between −80 mV and −5 mV was then divided by potassium driving force with a reversal potential of −100 mV. Peak conductance was then plotted against the voltage of the corresponding voltage step and was fitted with a Boltzmann function as follows:

$$I(V) = I_0 + \frac{I_{max}}{1 + \exp\frac{-(V - V_{50})}{b}}$$

where I_0 is basal current, I_{max} is the maximal current, V is voltage, V_{50} is half-activation voltage, and b scales the voltage sensitivity of activation/inactivation.

I_A V_{50} and I_A b were extracted from this analysis. I_A time constant of activation and inactivation were obtained using a diexponential fit (exponential rise to maximum and exponential decay) of the current. To assess I_A inactivation properties, 500 ms voltage steps were applied from −40 to −120 mV (in increments of −5 mV) followed by a 500 ms voltage step at −40 mV. Then, the peak current measured during the pulse to −40 mV was plotted against the voltage of the conditioning prepulses to obtain the inactivation curve of I_A. Data were fitted with a Boltzmann function (four-parameter sigmoidal function, see equation), and V_{50} and b were extracted from this analysis.

A two-step voltage-clamp protocol was used to determine the voltage-dependent activation of I_H. A prepulse to various holding potentials from −60 to −130 mV (increments of −5 mV associated with progressive decrements in step duration) was used to activate I_H to different extents. A subsequent pulse to −130 or −120 mV was used to measure the degree of activation of I_H independent of changes in driving force. Finally, the amplitude of I_H measured during the pulse to −130 or −120 mV was plotted against the voltage of the prepulse, and the data were fitted using the Boltzmann function equation. V_{50}, b, and I_H I_{max} were extracted from this analysis. I_H time constant of activation was obtained using single exponential fits of the current at the different voltage steps.

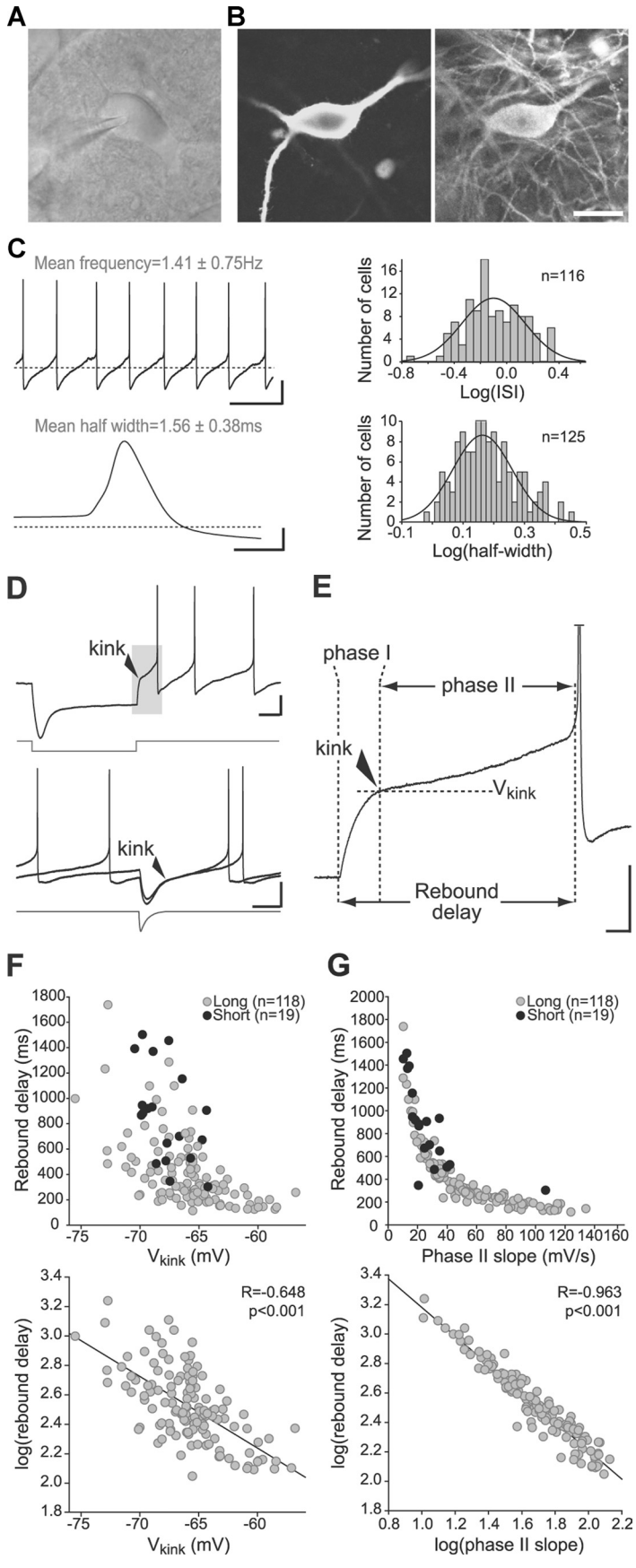

Figure 1. Identification of SNc dopaminergic neurons and dissection of rebound properties. ***A***, Infrared image of a dopaminergic neuron and the patch pipette. ***B***, Left, Fluorescent streptavidin labeling of a neuron filled with neurobiotin. Right, Tyrosine hydroxylase immunolabeling of the same neuron. ***C***, Characteristic electrophysiological properties of SNc dopaminergic neurons. Top row, Left, Current-clamp recording showing the typical pacemaker tonic firing of a dopaminergic neuron. Right, Histogram of the log-normal distribution of the interspike interval (inverse of the instantaneous frequency). Bottom row, Left, Current-clamp recording showing the typical slow action potential waveform of a dopaminergic neuron. Right, Histogram of the log-normal distribution of action potential half-width. Dashed lines indicate −60 mV. ***D***, Rebound waveform in SNc dopaminergic neurons. Top, Current-clamp recording of a typical response of a neuron to a 1 s hyperpolarizing current step leading to −120 mV, showing the clear kink in the repolarization. The gray trace represents the current step from 0 to −125 pA. Bottom, The rebound elicited by short diexponential synaptic-like pulses also displayed a biphasic repolarization. The gray trace represents the −287 pA current injection. ***E***, Expanded version corresponding to the gray box in ***D***. Two phases of repolarization (phase I, phase II) are distinguished based on the rate of repolarization. The transition point was named "kink" and the corresponding voltage V_{kink}. ***F***, Scatter plots summarizing the correlation between rebound delay and V_{kink}. Top, Scatter plot showing the relationship between rebound delay elicited by 1 s steps (gray circles) or short synaptic-like (black circles) hyperpolarizing stimuli. Bottom, Scatter plot illustrating the significant correlation between log (rebound delay) and V_{kink} for long hyperpolarizations (R, p, and n values are on the plot). ***G***, Scatter plots summarizing the correlation between rebound delay and phase II slope. Top, Scatter plot showing the relationship between rebound delay and phase II slope elicited by 1 s (gray circles) or short synaptic-like (black circles) hyperpolarizing pulses. Bottom, Scatter plot illustrating the significant correlation between log (rebound delay) and log (phase II slope) for long hyperpolarizations (R, p, and n values are on the plot). Scale bars: ***A***, ***B***, 20 μm. Calibration: ***C***, Top, 20 mV, 1 s; ***C***, Bottom, 20 mV, 2 ms; ***D***, Top, 20 mV, 200 ms; ***D***, Bottom, 20 mV, 200 ms; ***E***, 20 mV, 20 ms.

Dynamic-clamp recordings and analysis. To model I_H and I_A, all the parameters for the conductance definitions were extracted from our voltage-clamp recordings (see Tables 1, 2; Fig. 7). The voltage dependence of the time constant of I_H activation (I_H τ_m) was fitted with a four-parameter peak Gaussian equation (see Fig. 7*B*; $n = 27$, average fit) and the values of the holding potential at the peak of the Gaussian fit were extracted (see Tables 1, 2, V_τ) and plotted against the I_H activation V_{50} values. As there was a significant positive correlation between V_τ and I_H activation V_{50} (linear regression, $R = 0.84$, $p < 0.001$, $n = 27$), when I_H activation V_{50} was shifted in the modeled I_H, V_τ was shifted accordingly. The voltage dependencies of I_A time constant of activation (I_A τ_m) and inactivation (I_A τ_h) were fitted with a Boltzmann function (four-parameter sigmoidal function, see equation; $n = 19$; see Fig. 7*C*,*D*, average fit). However, there was no correlation between the I_A τ_m or I_A τ_h V_{50} values and the I_A activation and inactivation V_{50} values, respectively ($R = 0.07$, $p = 0.79$, $n = 19$; $R = 0.07$, $p = 0.81$, $n = 19$, respectively). Thus, for the model of I_A, I_A τ_m and I_A τ_h were not shifted in conjunction with the activation and inactivation curves of I_A. For the data presented in Figure 9*C*, values of injected maximum conductances (gm_A, gm_H)

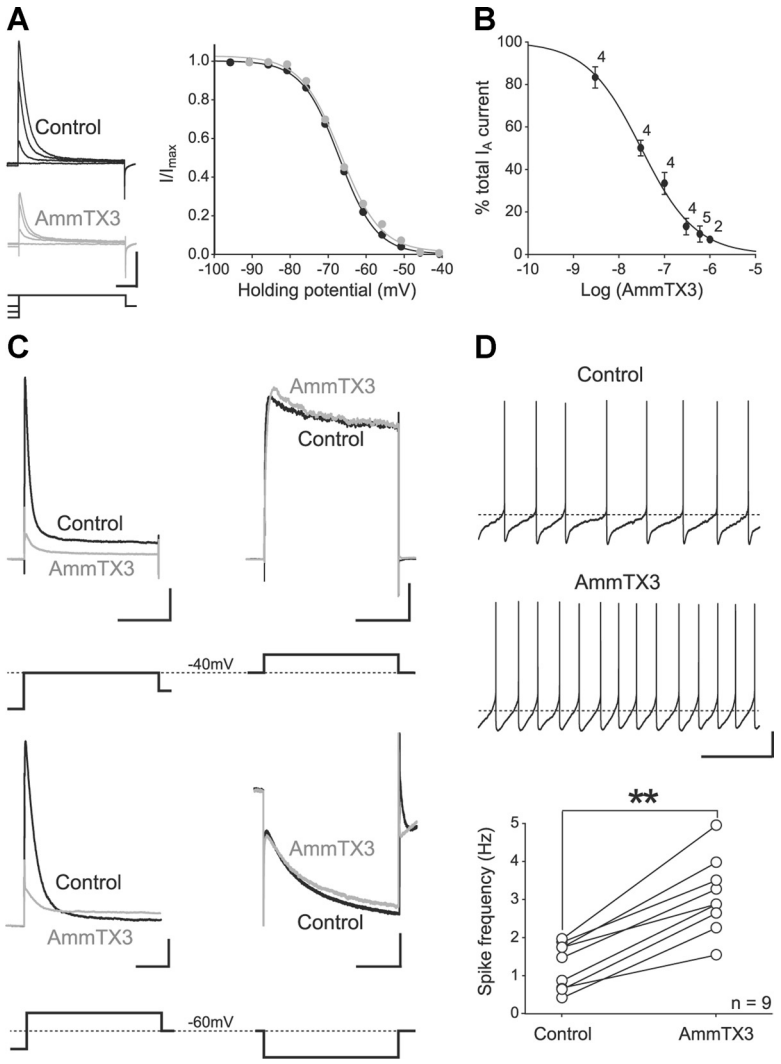

Figure 2. Characterization of AmmTX3 activity in SNc dopaminergic neurons. ***A***, AmmTX3 blocks I_A without modifying gating properties. Left, Voltage-clamp recordings of I_A (step to −40 mV from holding potentials of −40, −60, −70, and −80 mV shown beneath traces) obtained from the same neuron in control conditions (top, black traces) and in the presence of 100 nM AmmTX3 (bottom, gray traces). Right, Inactivation curves corresponding to the traces presented on the left. Note that AmmTX3 only reduces the amplitude of the current without modifying the inactivation properties. ***B***, Dose–response curve of the effect of AmmTX3 on I_A amplitude in SNc dopaminergic neurons in acute brain slices. Numbers above the points indicate the number of cells used for the quantification of the effect of the toxin at different concentrations. ***C***, 300–600 nM AmmTX3 blocks I_A but does not affect the delayed rectifier potassium current ($n = 5$) or I_H ($n = 4$). Top, Voltage-clamp recordings of I_A (left, step to −40 mV from a −100 mV prestep shown beneath traces) and the delayed rectifier potassium current (right, step to −10 mV from a −40 mV prestep shown beneath traces) from the same neuron in control (black traces) and in the presence of 300 nM AmmTX3 (gray traces). Bottom, Voltage-clamp recordings of I_A (left, step to −40 mV from a −100 mV prestep shown beneath traces) and I_H (right, step to −110 mV from a −60 mV prestep shown beneath traces) from the same neuron in control (black traces) and in the presence of 300 nM AmmTX3 (gray traces). Note that while I_A is almost completely abolished by toxin application, the potassium-delayed rectifier current and I_H are not affected. ***D***, AmmTX3 has the expected effect of I_A blockers on spontaneous pacemaker activity. Top and Middle, Current-clamp recordings of spontaneous activity in a neuron in control condition (top) and in the presence of 300 nM AmmTX3 (middle). Bottom, Scatter plot showing the significant increase in spontaneous frequency induced by 300 nM AmmTX3 in nine SNc dopaminergic neurons. Dashed lines indicate −60 mV (current-clamp) or 0 pA (voltage-clamp). $^{**}p < 0.01$. Calibration: ***A***, 2 nA, 100 ms; ***C***, Top right and left, 2 nA, 200 ms; ***C***, Bottom left, 1 nA, 100 ms; ***C***, Bottom right, 250 pA, 500 ms; ***D***, 20 mV, 2.5 s.

were normalized to the input conductance to account for the shunting effect of background membrane conductances on the efficiency of injected conductances. Input conductance was measured using a hyperpolarizing current-clamp pulse after complete blockade of I_A and I_H.

To inject the models of I_A and I_H, we used the SM-2 software developed by Hugh Robinson (Robinson, 2008) (Cambridge Conductance), which runs on a scriptable digital-signal-processing (DSP)-based system for dynamic conductance injection. Conductance definitions for I_H and I_A were compiled and downloaded from the PC to a P-25M DSP board (Innovative Integration), which executes the conductance injection with a sampling rate of 40 KHz over a 2 V range with a resolution of 0.1 mV.

Data acquisition and analysis. Data were acquired using an EPC 10 USB patch-clamp amplifier (HEKA) and the Patchmaster software acquisition interface (HEKA). Analysis was performed using FitMaster v2x30 (Heka) and Igor Pro (version 6.0, WaveMetrics). The statistical analysis, performed according to the distribution properties of the data, included linear regression, multiple linear regression, product moment (Pearson), rank order correlation (Spearman), unpaired *t* test, Mann–Whitney, paired *t* test, Fisher test (for variance comparison), one-way ANOVA, standard sigmoidal fitting procedure, and Gaussian fitting procedure (all conducted using SigmaPlot 10.0, Jandel Scientific), with $p < 0.05$ considered to be statistically significant. Figures were prepared using SigmaPlot, GraphPad Prism 5, Igor Pro, Photoshop CS4, and Adobe Illustrator CS4. Unless otherwise stated, data are presented as mean ± SEM in figures and as mean ± SD in the main text.

Results

Dissecting the rebound properties of SNc dopaminergic neurons

To investigate the roles of I_A and I_H in the rebound properties of SNc dopaminergic neurons, we first performed a detailed current-clamp analysis of these neurons in P16–P22 rat acute midbrain slices. SNc dopaminergic neurons were identified based on their location, size, and morphology (Fig. 1*A*) and their characteristic electrophysiological properties (Kita et al., 1986; Grace and Onn, 1989; Kitai et al., 1999) (Fig. 1*C*). In 72 of 73 cells, the dopaminergic identity was confirmed by *post hoc* tyrosine hydroxylase (a dopamine synthesis enzyme) immunolabeling (Fig. 1*B*). Consistent with the numerous studies performed on this preparation (Kita et al., 1986; Grace and Onn, 1989; Kitai et al., 1999; Nedergaard, 1999; Liss et al., 2001; Putzier et al., 2009), most dopaminergic neurons displayed low-frequency pacemaker activity (mean frequency, 1.41 ± 0.75 Hz, $n = 116$), with slow action potentials (mean half-width, 1.56 ± 0.38 ms, $n = 125$; Fig. 1*C*), and a characteristic response to long hyperpolarizing current steps consisting of a large voltage sag (>30 mV) during current injection and a biphasic repolarization after hyperpolarization is released (Fig. 1*D*). While the sag is thought to be essentially the consequence of the activation of I_H (Franz et al., 2000; Neuhoff et al., 2002), the biphasic rebound most likely reveals the influence of I_A at subthreshold potentials (Kita et al., 1986; Nedergaard, 1999). The rebound was separated into two successive phases based on its voltage trajectory (Fig. 1*E*): an immediate repolarization phase

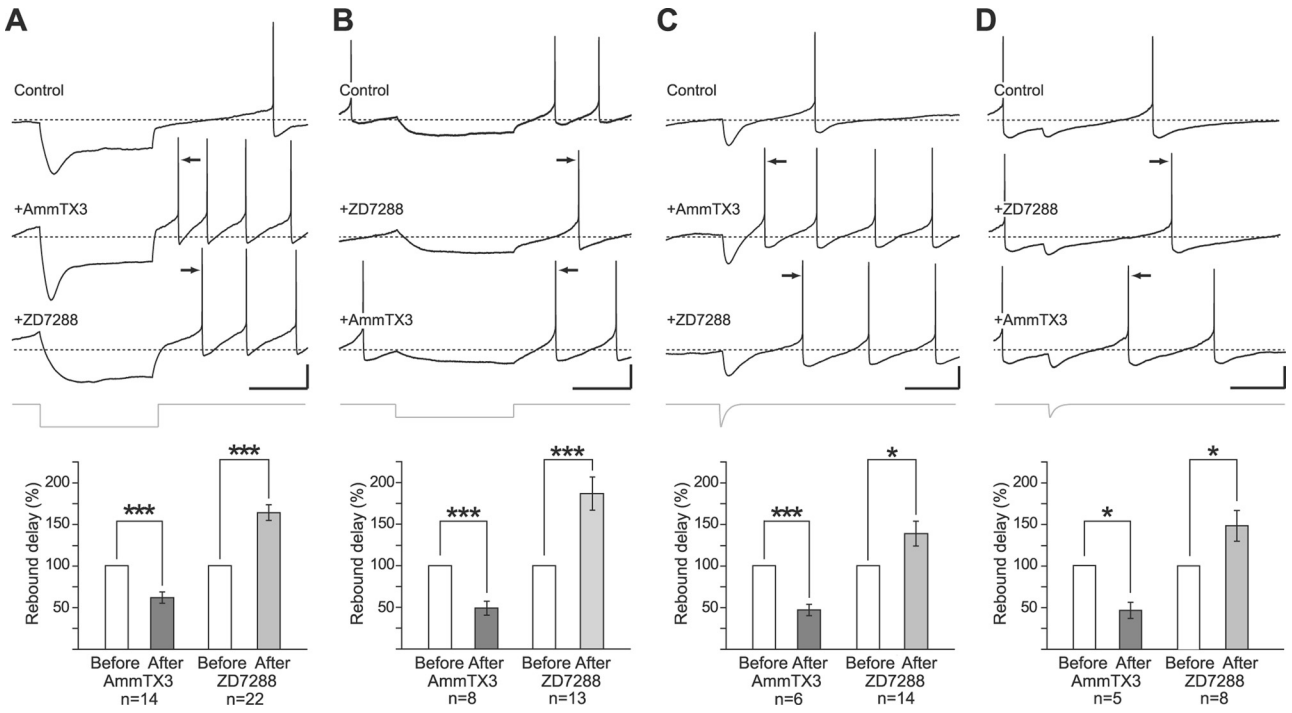

Figure 3. Effects of specific blockers of I_A and I_H on rebound properties. ***A***, Rebound response induced by a 1 s hyperpolarizing pulse (−84.0 mV at the end of the pulse) in control (top trace), in the presence of 300 nM AmmTX3 (middle trace), and in the presence of AmmTX3 + 3 μM ZD7288 (bottom trace). Bottom, Bar plot showing the average rebound delay values before and after the application of AmmTX3 and ZD7288. ***B***, Rebound response induced by a 1 s hyperpolarizing pulse (−71.9 mV at the end of the pulse) in control (top trace), in the presence of 3 μM ZD7288 (middle trace), and in the presence of ZD7288 + 300 nM AmmTX3 (bottom trace). Bottom, Bar plot showing the average rebound delay before and after the application of AmmTX3 and ZD7288. ***C***, Same experimental protocol as in ***A***, but using short synaptic-like hyperpolarizations (−84.9 mV at the peak) to induce the rebound. Bottom, Bar plot showing the average rebound delay before and after AmmTX3 and ZD7288 application. ***D***, Same experimental protocol as in ***B***, but using short synaptic-like hyperpolarizations (−71.9 mV at the peak) to induce the rebound. Bottom, Bar plot showing the average rebound delay values before and after AmmTX3 and ZD7288 application. The gray traces in ***A***–***D*** represent the current stimulus. $^*p < 0.05$, $^{**}p < 0.01$, $^{***}p < 0.001$. Dashed lines in traces indicate −60 mV. Calibration: ***A***–***D***, 20 mV, 500 ms.

after release from hyperpolarization (phase I) leading to a kink (V_{kink} is the membrane potential at this point), from which arises a slow repolarization phase (phase II), leading to spike threshold. While the duration of phase I was not correlated with rebound delay, both V_{kink} and the slope of repolarization during phase II (phase II slope) showed significant correlations with rebound delay [V_{kink} vs log(rebound delay), $R = -0.648$, $p < 0.001$, $n = 118$; log(phase II slope) vs log(rebound delay), $R = -0.963$, $p < 0.001$, $n = 118$, Pearson; Fig. 1*F*,*G*]. V_{kink} and phase II slope also shared a significant positive correlation, such that phase II slope increased when V_{kink} depolarized [log(phase II slope) vs V_{kink}, $R = 0.592$, $p < 0.001$, $n = 138$, Pearson], suggesting that these two parameters may be mediated by common mechanisms.

Although long hyperpolarizing current steps such as those used here (1 s duration, leading to voltages of −84.0 ± 1.8 mV at the end of the pulse) constitute the typical protocol used to analyze rebound properties (Harris-Warrick et al., 1995; Neuhoff et al., 2002), we wanted to determine whether such rebound behavior could be triggered by more "physiological" stimuli. As GABAergic synaptic inputs represent >70% of the total number of synaptic inputs received by SNc dopaminergic neurons (Tepper and Lee, 2007), we also used short current injections reproducing the waveform of a GABAergic IPSC (Tanaka et al., 2009; scaled to reach a peak hyperpolarization of −84.9 ± 2.1 mV; Fig. 1*D*). Although these events were shorter and induced a milder hyperpolarization than the 1 s current step, they triggered a very similar biphasic rebound (Fig. 1*D*). Moreover, the quantitative relationships between V_{kink}, phase II slope, and rebound delay for the short synaptic-like hyperpolarizations lay along the same distribution as those observed for long hyperpolarizations (Fig. 1*F*,*G*).

I_A and I_H have opposite and complementary effects on rebound firing

To determine the precise contribution of I_A and I_H to the rebound properties, we tested the effect of specific blockers of the channels underlying these currents in dopaminergic neurons. In SNc dopaminergic neurons, I_A and I_H are carried by the long isoform of the potassium Kv4.3 channel (Liss et al., 2001; Hahn et al., 2003) and by subunits 2, 3, and 4 of the hyperpolarization-activated cyclic nucleotide-gated (HCN) channels, respectively (Franz et al., 2000; Neuhoff et al., 2002). While ZD7288 was used to block I_H (Neuhoff et al., 2002; Chan et al., 2007), we used the scorpion toxin AmmTX3, a pore-blocker for the Kv4 channel family (Vacher et al., 2002, 2004), to block I_A (Fig. 2). In SNc dopaminergic neurons, nanomolar concentrations of AmmTX3 selectively blocked I_A and increased spontaneous pacemaking frequency (Fig. 2, $p < 0.01$, $n = 9$, paired *t* test), as expected for I_A blockers in these cells (Nedergaard, 1999; Liss et al., 2001; Putzier et al., 2009). We used nonsaturating concentrations of AmmTX3 (300 nM) and ZD7288 (3 μM), which suppress 60–85% of either current but did not disrupt the characteristic biphasic waveform of the rebound (Fig. 3). AmmTX3 and ZD7288 were applied consecutively to neurons in randomized order. As their effects were consistent with respect to the induced changes in rebound delay, phase II slope, and V_{kink} for all hyperpolarizing protocols independent of the order in which they were applied, the

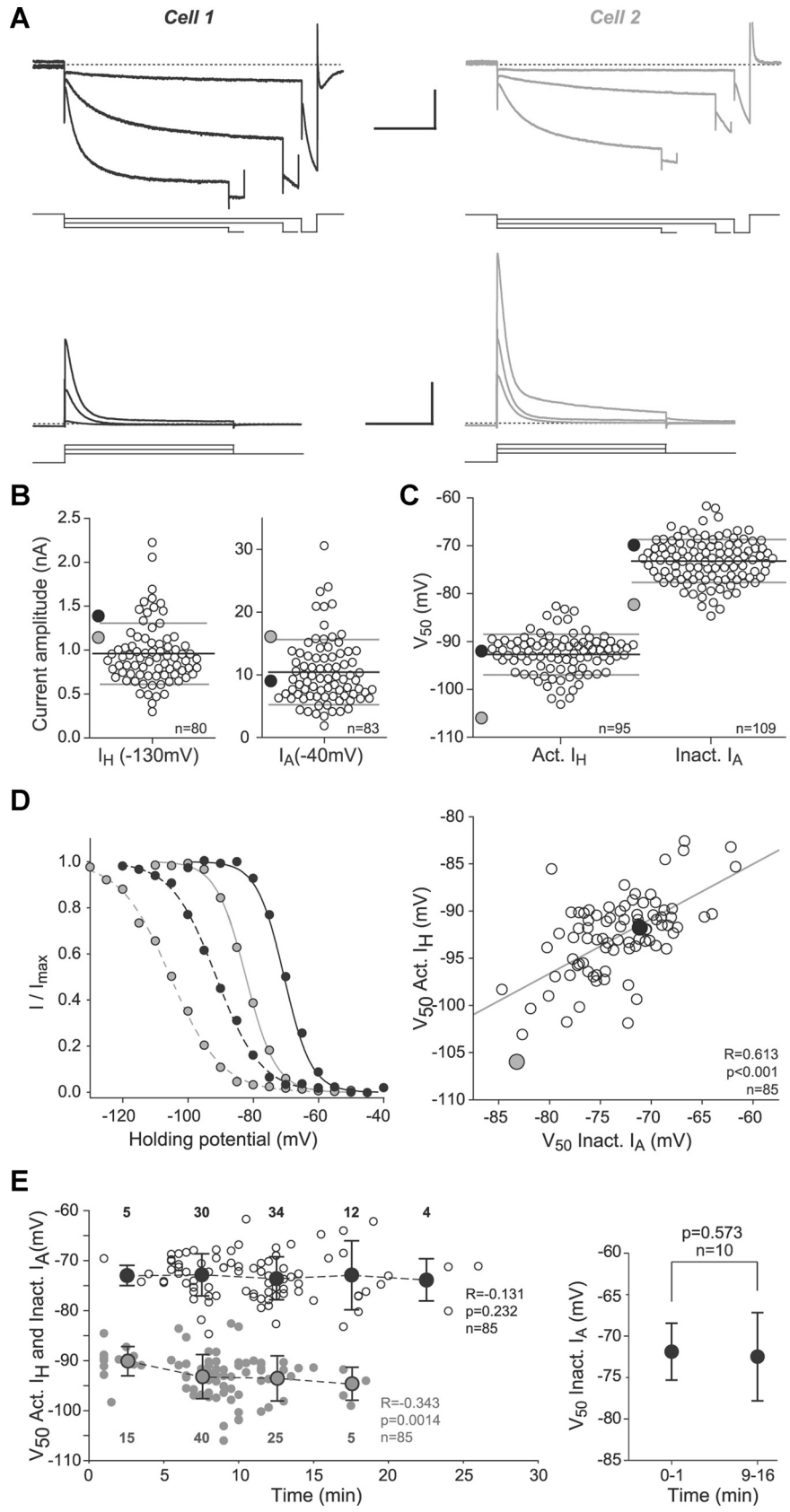

Figure 4. Variability and covariation of I_A and I_H biophysical properties. ***A***, Top, Voltage-clamp recordings of I_H in two dopaminergic neurons in response to hyperpolarizing pulses at −80, −100, and −120 mV from a holding potential of −60 mV, followed by a pulse at −130 mV. Bottom, Voltage-clamp recordings of I_A in the same cells in response to a depolarizing pulse to −60, −50, and −40 mV from a holding potential of −100 mV. Dashed lines indicate 0 pA. ***B***, Scatter plots showing the variability in amplitude of I_H maximum current recorded at −130 mV (left) and I_A recorded at −40 mV (right). Black and gray lines indicate the mean and SD, respectively. ***C***, Scatter plots showing the variability in the voltage dependence of activation of I_H (left) and inactivation of I_A (right). Black and gray lines indicate the mean and SD, respectively. ***D***, Left, I_H activation (dashed line) and I_A inactivation (solid line) curves corresponding to the cells presented in ***A***. Right, Scatter plot showing the significant positive correlation between I_H activation and I_A inactivation V_{50} values. In ***B***–***D***, the black and gray circles correspond to the voltage-clamp recordings of the two neurons presented in ***A***. ***E***, Left, Scatter plot showing the relationships between the time after breaking into whole-cell configuration and I_A inactivation (small empty circles) or I_H activation (small gray circles) V_{50} values for the cells presented in Figure 4*D*, right. Large circles represent the average values of I_A inactivation (black) and I_H activation (gray) V_{50} values for each 5 min time window following break-in to whole-cell configuration (the *n* for each 5 min time window is indicated at the top and bottom of the plot). Note the lack of a significant correlation between I_A inactivation V_{50} values and time following break-in, and the significant correlation between the time following break-in and I_H activation V_{50} values (*R*, *p*, and *n* values are indicated on the plot). Right, Plot showing no change between the average I_A inactivation V_{50} values in the same cells ($n = 10$) recorded immediately after obtaining whole-cell configuration (0–1 min) and again after 9–16 min. Calibration: ***A***, Top, 500 pA, 2 s; Bottom, 4 nA, 200 ms. Error bars represent SD.

data were pooled into before and after AmmTX3/ZD7288 application datasets.

ZD7288 and AmmTX3 induced opposite changes in rebound firing in response to both long and short synaptic-like hyperpolarizations leading to voltages of −84.0 at the end and −84.9 at the peak of the pulse, respectively (Fig. 3*A*,*C*). When using long hyperpolarizing steps, AmmTX3 significantly decreased rebound delay ($p < 0.001$, $n = 14$, paired *t* test), increased phase II slope ($p = 0.007$, $n = 9$, paired *t* test), and depolarized V_{kink} ($p = 0.001$, $n = 9$, paired *t* test), while ZD7288 significantly delayed rebound firing ($p < 0.001$, $n = 22$, paired *t* test), decreased phase II slope ($p < 0.001$, $n = 18$, paired *t* test), and hyperpolarized V_{kink} ($p = 0.003$, $n = 18$, paired *t* test; Fig. 3*A*; see Fig. 8*D*), consistent with previous observations (Neuhoff et al., 2002). These effects were consistent with the correlations between V_{kink}, phase II slope, and rebound delay described earlier (Fig. 1*F*,*G*). AmmTX3 and ZD7288 also significantly decreased ($p < 0.001$, $n = 6$, paired *t* test) and increased ($p = 0.023$, $n = 14$, paired *t* test) rebound delay, respectively, after short synaptic-like hyperpolarizations (Fig. 3*C*). As the hyperpolarizing protocols used so far could potentially enhance I_H involvement in the rebound responses, we also induced rebound firing using hyperpolarizations that resulted in voltages of −71.9 ± 1.3 and −71.9 ± 1.5 mV at the end of the pulse for long hyperpolariza-

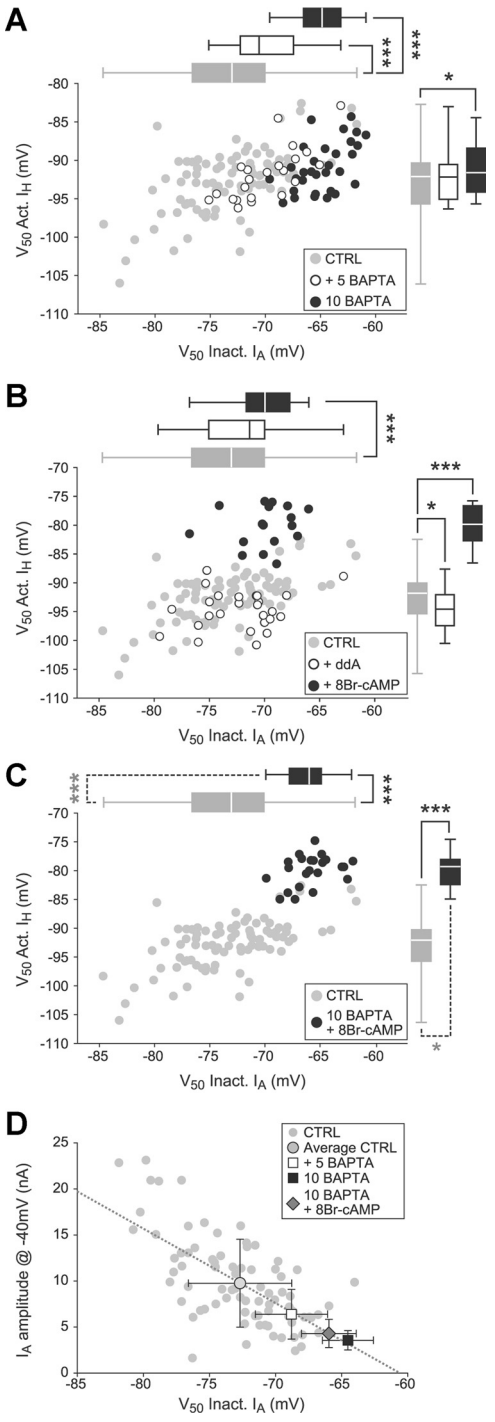

Figure 5. I_A and I_H covariation of voltage dependences is sensitive to cytosolic calcium and cAMP concentrations. ***A***, Scatter and box plots illustrating the effect of BAPTA on I_H activation and I_A inactivation voltages. Compared with the control population (***A–C***, gray circles/boxes; $n = 109$ and 95 for I_A inactivation and I_H activation V_{50} values, respectively), the addition of 5 mM BAPTA to the patch pipette (white circles/boxes) significantly depolarizes the inactivation V_{50} of I_A ($n = 22$), but not the activation V_{50} of I_H ($n = 22$). The replacement of EGTA with 10 mM BAPTA in the patch pipette (black circles/boxes) significantly depolarizes both I_A inactivation and I_H activation V_{50} values ($n = 38$ and 35, respectively). ***B***, Scatter and box plots showing the effects of ddA and 8-Br-cAMP on I_A inactivation and I_H activation V_{50} values. ddA (white circles/boxes) significantly hyperpolarized I_H activation V_{50} ($n = 22$), but did not significantly shift I_A inactivation V_{50} ($n = 28$). 8-Br-cAMP (black circles/boxes) significantly depolarized both I_A inactivation ($n = 21$) and I_H activation ($n = 17$) V_{50} values. ***C***, Scatter and box plots illustrating the effect of the coapplication of 10 mM BAPTA and 8-Br-cAMP on I_A inactivation and I_H activation V_{50} values. Data show that 10 mM BAPTA/8-Br-cAMP (black circles/boxes) significantly depolarized I_A inactivation ($n = 24$) and I_H activation ($n = 22$) V_{50} values (black asterisks), and also significantly reduced the variability (gray asterisks, *F* test) for both I_A inactivation and I_H activation V_{50} values compared with the control population. ***D***, Scatter plot illustrating the negative linear regression ($R = -0.663$, $p < 0.001$) present between I_A inactivation V_{50} and the amplitude of I_A measured at −40 mV in the control population (gray circles), and the alignment of the average values for the control population (large gray circle), 5 mM BAPTA (white square), 10 mM BAPTA (black square), and 10 mM BAPTA/8-Br-cAMP conditions (gray diamond) along this regression line. Box-and-whisker plots in ***A–C*** represent the median value and first and third quartiles (box), and the minimum and maximum values of the distribution (whiskers). Error bars in ***D*** represent SD. *$p < 0.05$, **$p < 0.01$, ***$p < 0.001$.

tions and at the peak for the short hyperpolarizations, respectively (Fig. 3*B*,*D*). These milder hyperpolarizations are equivalent to the trough voltage recorded during spontaneous pacemaking (-72.1 ± 4.4 mV, $n = 162$) and induce a weaker activation of I_H (Fig. 3*B*,*D*). Even in these conditions, AmmTX3 and ZD7288 significantly decreased and increased rebound delay, respectively, for both long ($p < 0.001$, $n = 8$, paired *t* test; $p < 0.001$, $n = 13$, paired *t* test) and short hyperpolarizations ($p < 0.05$, $n = 5$, paired *t* test; $p < 0.05$, $n = 8$, paired *t* test; Fig. 3*B*,*D*). Moreover, the magnitude of the effects of ZD7288 and AmmTX3 on rebound delay was not statistically different between the −84 and −72 mV long and short hyperpolarization protocols (one-way ANOVA; $p = 0.24$, $p = 0.40$, respectively; Fig. 3). These results confirm that common biophysical mechanisms involving predominantly I_A and I_H underlie rebound firing, and suggest that I_A and I_H complementarity may be involved in physiological responses to inhibitory inputs.

Variability and correlations in the biophysical properties of I_A and I_H

To determine the biophysical basis of the strong functional complementarity of I_A and I_H, we measured the amplitude, voltage dependence, and kinetics of I_H and I_A in 109 SNc dopaminergic neurons. We first observed that dopaminergic neurons exhibit widely different I_A and I_H amplitudes and voltage dependences (Fig. 4*A–C*). While variability in the amplitude of currents (Fig. 4*B*) has already been described for various currents in many systems (including I_A and I_H in SNc neurons) (Liss et al., 2001; Golowasch et al., 2002; Neuhoff et al., 2002; MacLean et al., 2005; Swensen and Bean, 2005; Schulz et al., 2006, 2007; Khorkova and Golowasch, 2007; Goaillard et al., 2009; Temporal et al., 2011), we found that other properties, such as voltage dependence, can also display a high degree of variability from cell to cell (Fig. 4*C*). The variability in voltage dependence [represented by the activation and inactivation midpoints (V50)] and amplitude was independent of age (age vs I_H activation V_{50} or I_A inactivation V_{50}: $R = -0.164$, $p = 0.098$, $n = 104$, Pearson; or $R = -0.24$, $p = 0.168$, $n = 125$, Pearson; age vs I_H or I_A amplitude: $R = -0.07$, $p = 0.48$, $n = 84$, Spearman; or $R = 0.058$, $p = 0.747$, $n = 33$, Spearman, respectively) and of the input resistance of the neurons (input resistance vs I_H activation V_{50} or I_A inactivation V_{50}: $R = 0.114$, $p = 0.294$, $n = 86$, Spearman; or $R = 0.0852$, $p = 0.38$, $n = 108$, Spearman; input resistance vs I_H or I_A amplitude: $R = -0.0543$, $p = 0.647$, $n = 73$, Spearman; or $R = -0.227$, $p = 0.226$, $n = 30$, Spearman, respectively). Various studies have shown that the inactivation and activation properties of the Kv4 channels can be regulated either independently (Anderson et al., 2010) or in a coordinated manner (Hoffman and Johnston, 1998; Yu et al., 1999; Levy et al., 2010). We measured I_A activation properties in a subset of neurons ($n = 32$) and found that the half-inactivation and the half-activation voltages of I_A were positively correlated ($R = 0.418$, $p = 0.017$, Pearson). Consistent

←

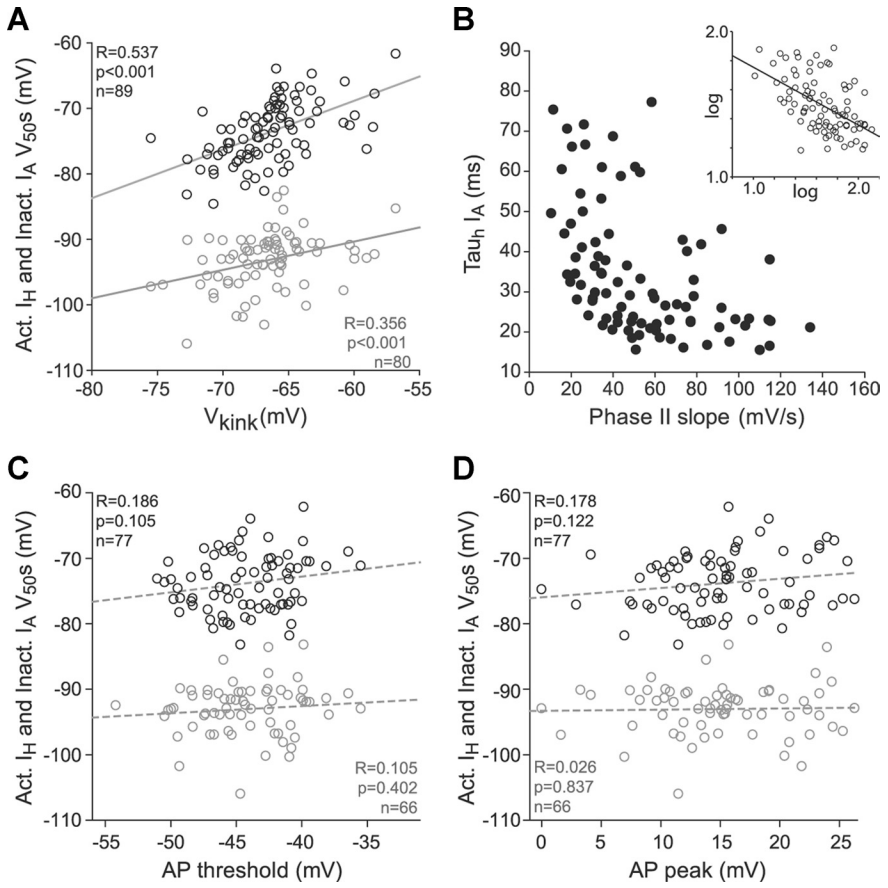

Figure 6. Summary of correlations between I_A and I_H biophysical properties and firing parameters. ***A***, Scatter plot showing the significant positive correlations between the V_{kink} and I_A inactivation (black) and I_H activation (gray) V_{50} values. Gray lines indicate the linear regressions for I_A and I_H V_{50} values (R, p, and n values are at the top left and bottom right of the plot), respectively. ***B***, Scatter plot illustrating the significant correlation between I_A τ_h and phase II slope. The gray line (inset) indicates the linear regression between the log transforms of the variables. ***C***, Scatter plot representing the absence of correlations between action potential threshold and I_A (black) and I_H (gray) V_{50} values. The dashed gray line indicates the linear regressions (R, p, and n values are on the plot). ***D***, Scatter plot representing the absence of correlations between action potential peak and I_A (black) and I_H (gray) V_{50} values. The dashed gray line indicates the linear regressions (R, p, and n values are on the plot).

with the coordinated shift in I_A inactivation and activation V_{50} values, I_A amplitude measured at −40 mV was found to be negatively correlated with I_A inactivation V_{50} in the whole population (Fig. 5*D*, gray circles; $R = -0.614$, $p < 0.001$, $n = 83$, Spearman), as less current is generated at a given potential when the activation curve shifts toward depolarized potentials.

We then wondered whether the functional complementarity between I_A and I_H could emerge from the coregulation of some of their biophysical properties. Studies mostly performed on invertebrates have shown that the amplitude of I_A and I_H or the levels of expression of the channels carrying I_A and I_H are positively correlated in various cell types (MacLean et al., 2005; Schulz et al., 2007; Tobin et al., 2009; Cao and Oertel, 2011). As the large amplitude of I_A (>20 nA) in SNc dopaminergic neurons prevents an accurate measurement of the maximum conductance of the current in most SNc dopaminergic neurons, we were able to determine the maximum conductances of both I_A and I_H in a small subset of neurons ($n = 23$), and did not observe a statistically significant correlation between these parameters ($R = 0.258$, $p = 0.242$, $n = 22$, Spearman). Surprisingly, though, measuring I_H activation properties and I_A inactivation properties revealed that their voltage dependences were positively correlated ($R = 0.613$, $p < 0.001$, $n = 85$, Pearson; Fig. 4*D*). In addition, there was also a significant positive correlation between I_H activation V_{50} and I_A activation V_{50} ($R = 0.459$, $p = 0.0315$, $n = 22$, Spearman). When the time of recording following breaking into whole-cell configuration was compared with I_A inactivation V_{50}, there was no significant change over time ($R = 0.131$, $p = 0.232$, $n = 85$, Spearman; Fig. 4*E*). Rundown experiments verified that I_A inactivation V_{50} values did not change over time during whole-cell recording in the same cells: I_A was measured immediately following break-in and again after 9–16 min ($p = 0.573$, $n = 10$, paired t test; Fig. 4*E*). However, there was a small but significant hyperpolarization of I_H activation V_{50} over time (−0.32 mV/min, $R = 0.343$, $p = 0.001$, $n = 85$, Spearman; Fig. 4*E*), as has been previously reported (Zolles et al., 2006). Nevertheless, significant variability was present for I_H activation and I_A inactivation V_{50} values recorded within 5 min of obtaining whole-cell configuration (Fig. 4*E*). Importantly, despite the slight hyperpolarization of I_H over time, there was a significant correlation between I_H and I_A V_{50} values in subsamples of cells from narrow time windows at the beginning (1–7.5 min, $R = 0.673$, $p < 0.001$, $n = 31$, Spearman), middle (8–11 min, $R = 0.532$, $p = 0.0013$, $n = 34$, Spearman), or end (11.5–19 min, $R = 0.692$, $p < 0.001$, $n = 20$, Spearman) of the time range. These data demonstrate that cytoplasmic dialysis was not responsible for the variability of I_A inactivation and I_H activation V_{50} values or their covariation.

I_H and I_A covariation of voltage dependences is sensitive to cAMP and calcium levels

We then considered the potential molecular machinery underlying the I_A and I_H covariation in voltage dependences. Kv4.3 channels in the SNc dopaminergic neurons are associated with the calcium-sensitive auxiliary subunit KChip3.1 (Liss et al., 2001). Thus, I_A properties might be modulated by calcium variations (An et al., 2000), as has been demonstrated in other cell types (Patel et al., 2002; Anderson et al., 2010). Furthermore, two of the three subunits responsible for I_H in SNc dopaminergic neurons (HCN2 and HCN4; Franz et al., 2000) are very sensitive to cAMP variations (Biel et al., 2009), and two out of the three adenylyl cyclases detected in the SNc dopaminergic neurons are inhibited by calcium (Chan et al., 2007). Therefore, we investigated whether locking intracellular calcium and cAMP levels could induce a coordinated shift of I_A and I_H voltage dependences and/or reduce the variability of their covariation.

Cells recorded with the fast calcium chelator BAPTA (5 mM) added to the control intracellular solution exhibited I_A inactivation V_{50} values slightly depolarized compared with the control population (average of −69.91 ± 3.07 vs −73.18 ± 4.48, $p < 0.001$, $n = 22$ vs $n = 109$, Mann–Whitney), but no significant change in I_H activation V_{50} values ($p = 0.64$, $n = 22$ vs $n = 95$,

Mann–Whitney; Fig. 5*A*). However, using an intracellular solution containing 10 mM BAPTA and no EGTA resulted in a larger depolarization of I_A inactivation V_{50} (-64.81 ± 2.13 vs -73.18 ± 4.48, $p < 0.001$, $n = 38$ vs $n = 109$, unpaired t test) and a slight but significant depolarization of I_H activation V_{50} (-90.78 ± 3.16 vs -92.72 ± 4.24, $p = 0.015$, $n = 35$ vs $n = 95$, unpaired t test; Fig. 5*A*). Interestingly, the I_A inactivation V_{50} values measured in 10 mM BAPTA were located within the range recorded in control condition, but clustered at the depolarized edge of the range.

To manipulate the cytosolic cAMP levels, we first used a nonselective adenylyl cyclase inhibitor ddA (20 μM) to induce a decrease in cAMP concentration (Chan et al., 2007). While ddA induced a significant hyperpolarization of I_H activation V_{50} values (-94.8 ± 3.55 vs -92.72 ± 4.24, $p = 0.0186$, $n = 22$ vs $n = 95$, Mann–Whitney), I_A inactivation V_{50} values were unaffected ($p = 0.19$, Mann–Whitney; Fig. 5*B*). We then used the nondegradable cAMP analog 8-Br-cAMP (25 μM) to artificially increase the cytosolic cAMP level, resulting in a significant depolarization of both I_H activation V_{50} (-80.23 ± 3.5 vs -92.72 ± 4.24, $p < 0.001$, $n = 17$ vs $n = 95$, Mann–Whitney) and I_A inactivation V_{50} values (-69.99 ± 2.58 vs -73.18 ± 4.48, $p < 0.001$, $n = 21$ vs $n = 109$, Mann–Whitney; Fig. 5*B*).

These experiments demonstrate that I_A and I_H are affected by changes in both cytosolic calcium and cAMP, with I_A being more sensitive to calcium manipulation while I_H is more sensitive to cAMP manipulation. As dopaminergic SNc neurons possess the molecular machinery to enable cross talk between the cAMP and calcium signaling pathways (Chan et al., 2007), we also tested the effect of combining 10 mM BAPTA with 8-Br-cAMP. This condition resulted in a dramatic depolarization of both I_A inactivation V_{50} (-65.96 ± 2.07 vs -73.18 ± 4.48, $p < 0.001$, $n = 24$ vs $n = 109$, Mann–Whitney) and I_H activation V_{50} (-80.12 ± 2.69 vs -92.72 ± 4.24, $p < 0.001$, $n = 24$ vs $n = 95$, Mann–Whitney; Fig. 5*C*). Most interestingly, combining BAPTA and 8-Br-cAMP was associated with a significant reduction in the variability of I_A inactivation (Fisher test to compare variances, $F = 4.7$, $p < 0.001$) and I_H activation ($F = 2.49$, $p = 0.015$) V_{50} values (Fig. 5*C*), effectively restricting the covariation of I_H and I_A voltage dependencies to a small region of the parameter space. While the values recorded in control condition covered a range of 23.0 and 23.4 mV for I_A inactivation and I_H activation V_{50} values, respectively, the values recorded in BAPTA plus 8-Br-cAMP were clustered in a range of 7.9 and 10.2 mV, respectively. Moreover, these values aligned with the distribution of values recorded in the control population. These data strongly suggest that the variabil-

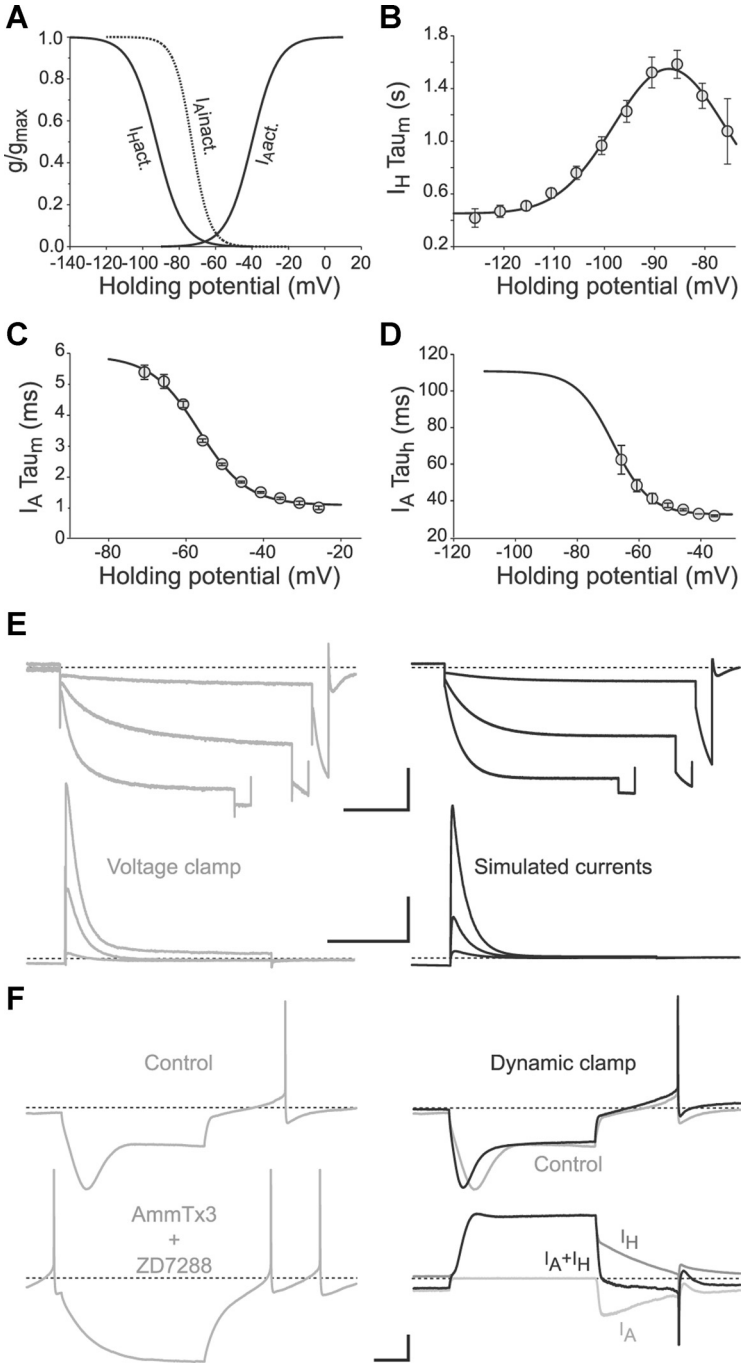

Figure 7. Dynamic-clamp simulation of I_A and I_H reproduces rebound profile. ***A***, Activation curves of I_H and I_A and inactivation curve of I_A from the biological currents used for the dynamic clamp. ***B***, Voltage dependence of the time constant of activation of I_H. The black line indicates the Gaussian fit of the experimental measures of the time constant of activation of I_H (gray circles, $n = 27$) used for the dynamic-clamp model. ***C***, ***D***, Voltage dependence of the time constants of activation (***C***) and inactivation (***D***) of I_A. The black line indicates the sigmoidal fit of the experimental values (gray circles, $n = 19$) used for the dynamic-clamp model. ***E***, Experimental traces (gray) and dynamic-clamp simulation (black) of I_H (voltage steps to -80, -100, -120 mV from -60 mV) and I_A (steps to -60, -50, -40 mV from -100 mV). ***F***, Current-clamp recordings showing the rebound profile of a neuron in control condition (gray trace, top left and right), after complete blockade of I_A and I_H (2 μM AmmTX3, 30 μM ZD7288, bottom left), and after injection of the simulated I_A and I_H (black trace, top right). Bottom right, Dynamic-clamp I_H (upper gray trace) and I_A (lower gray trace) currents injected into the neuron during the rebound protocol. The black trace (bottom right) corresponds to the sum of the two currents. Dashed lines indicate -60 mV (current-clamp) or 0 pA (voltage clamp, dynamic clamp). Calibration: ***E***, Top, 500 pA, 2 s; *E*, Bottom, 2 nA, 200 ms; ***F***, 20 mV/100 pA, 250 ms. See Table 1.

ity in I_H and I_A V_{50} values is partly due to the cell-to-cell variability in the local levels of calcium and cAMP. Additionally, this observation demonstrates that the large variability in I_H and I_A voltage dependences in control condition is not a consequence of uncompensated offsets, as this measurement error would be independent of pharmacological agents. Interestingly, the depolarization and restricted variability of the values obtained in BAPTA plus 8-Br-cAMP were not associated with an increase in input resistance compared with control, therefore ruling out space-clamp errors as the source of variability in voltage dependence of I_A and I_H. Furthermore, in experimental conditions in which I_A inactivation was significantly depolarized (5 mM BAPTA, 10 mM BAPTA, BAPTA plus 8-Br-cAMP), the amplitude of I_A measured at −40 mV was also significantly reduced, consistent with a coordinated depolarization of both I_A activation and inactivation curves (Fig. 5*D*). Although other signaling pathways may be involved in the modulation of I_A and I_H biophysical properties, these experiments demonstrate that the covariability of I_A and I_H voltage dependences is sensitive to local calcium and cAMP levels.

I_H and I_A biophysical properties quantitatively determine rebound properties

What is the relationship between the different phases of the rebound and the biophysical properties of I_A and I_H? Since rebound firing and the properties of I_A and I_H were measured in the same neurons, we were able to determine whether specific properties of these currents correlated with rebound parameters. Both I_A inactivation and I_H activation V_{50} values positively correlated with V_{kink} (Fig. 6*A*, Pearson), while the I_A time constant of inactivation (I_A τ_h) negatively correlated with phase II slope ($R = -0.533$, $p < 0.001$, $n = 88$; Fig. 6*B*, Pearson performed on log transforms of the variables) and with rebound delay ($R = 0.511$, $p < 0.001$, $n = 72$, Pearson on log transforms). However, both I_A inactivation and I_H activation V_{50} values were not correlated with the action potential threshold ($R = 0.186$, $p = 0.105$, $n = 77$, Pearson, and $R = 0.105$, $p = 0.402$, $n = 66$, Pearson, respectively; Fig. 6*C*) or peak voltage ($R = 0.178$, $p = 0.122$, $n = 77$, Pearson; or $R = 0.0259$, $p = 0.837$, $n = 66$, Pearson, respectively; Fig. 6*D*). The lack of correlation between the voltage dependences of I_H and I_A and other voltage properties in the same cells is also important as it rules out the possibility that uncompensated voltage offsets might be responsible for the covariations in I_H and I_A voltage dependences. Although these results suggest that the variations in I_A and I_H biophysical properties may modulate the rebound profile, they do not demonstrate a causal relationship.

Thus, we used the dynamic-clamp technique to determine whether these correlations between I_A and I_H biophysical properties and the rebound parameters represented causal relationships. The dynamic-clamp-simulated I_A and I_H were injected into neurons after complete blockade of the endogenous I_A and I_H by saturating concentrations of AmmTX3 (2 μM) and ZD7288 (30 μM; Fig. 7*F*). All the parameters used in the dynamic-clamp experiments were extracted from the voltage-clamp measurements presented in Figure 4 (Fig. 7*A–D*; Tables 1, 2). It is important to note that no specific adjustment of biophysical parameters was performed to reproduce the effects of the currents on rebound firing. The traces in Figure 7*E* show that these parameters precisely reproduced the voltage-clamp recordings obtained for the biological currents. Using these nonadjusted parameters also accurately reproduced the rebound behavior observed in unperturbed SNc dopaminergic neurons (Fig. 7*F*). Indeed, simulating the average parameters of I_A and I_H yielded V_{kink} and phase II slope values very similar to the average values observed in current-clamp in unperturbed neurons ($V_{kink} = -66.87 \pm 1.0$ vs -66.4 ± 3.9 mV, $n = 10$ vs $n = 118$, $p = 0.31$, Mann–Whitney; phase II slope = 62.72 ± 8.99 vs 57.4 ± 23.9 mV/s, $n = 10$ vs $n = 118$, $p = 0.13$, Mann–Whitney). This is particularly interesting since one of the drawbacks of the dynamic-clamp technique is that the simulated conductances are injected at a single point (in our case, the soma). If the currents characterized in voltage-clamp are mostly located far from the soma, space-clamp errors will contaminate the voltage-clamp measurements, and the simulation of these erroneous currents with dynamic clamp will not accurately reproduce the firing behavior observed in current-clamp in the unperturbed neurons (Storm et al., 2009). Our results argue that the biophysical properties of I_A and I_H in dopaminergic neurons can be accurately determined using whole-cell somatic recordings, and their influence on firing can be accurately tested using somatic dynamic clamp. Consistent with this, immunohistochemical labeling (Liss et al., 2001; and in our laboratory, data not shown) and voltage-clamp recordings from nucleated patches (Liss et al., 2001) and dissociated neurons (Puopolo et al., 2007) have also unambiguously demonstrated that I_H and I_A currents are present at high densities at the soma of SNc dopaminergic neurons. Moreover, since highly nonlinear relationships cannot be captured by averaging data (Golowasch et al., 2002; Marder and Taylor, 2011), reproducing the average firing behavior with dynamic-clamp-simulated average I_A and I_H suggests that the correlations between the biophysical properties of these currents are mostly linear or close to linearity.

Table 1. Equations and parameters used for the dynamic-clamp models of I_A and I_H

General equations	Current	$I(V,t) = gm_i * m(V,t) * h(V,t) * (V - E_{rev})$
	m_∞	$m_\infty(V) = 1/(1 + \exp[(V - V_{50m})/b])$
	h_∞	$h_\infty(V) = 1/(1 + \exp[(V - V_{50h})/c])$
	dm/dt	$dm(V,t)/dt = [m_\infty(V) - m(V,t)]/\tau_m(V)$
	dh/dt	$dh(V,t)/dt = [h_\infty(V) - m(V,t)]/\tau_h(V)$
I_H variables	m_∞	V_{50m}, $b = -7.25$
	τ_m (ms)	$\tau_m(V) = 456.5 + 1097.2 * \exp(-0.5 * [(V_\tau)/11.06]^2)$
	h_∞	1
	E_{rev} (mV)	−40
	gm_H (nS)[a]	13.9
I_A variables	m_∞	V_{50m}, $b = 7$
	τ_m (ms)	$\tau_m(V) = 1.029 + [4.83/(1 + \exp[(V + 56.7)/6.22])]$
	$\tau_{m,slow}$ (ms)	$\tau_m(V) = 1.543 + [7.25/(1 + \exp[(V + 56.7)/6.22])]$
	h_∞	V_{50h}, $c = -4.9$
	$\tau_{h,slow}$ (ms)	$\tau_h(V) = 58.6 + [117.57/(1 + \exp[(V + 68.5)/5.95])]$
	E_{rev} (mV)	−100
	gm_A (nS)[a]	316.8

[a]The values given for gm_A and gm_H correspond to 100% of the gm_A and gm_H used in the dynamic-clamp simulation of partial inhibition of I_H and I_A (Fig. 8). These values were also used for the experiments of covariation of voltage dependences. To assess the effects of varying the ratio of the two maximum conductances on the rebound, we used a range of 20–240% of the gm_A and gm_H values.

Table 2. Covariation of IA and IH voltage dependences

	Mean I_H Mean I_A (2)	Hyp. I_H Hyp. I_A (3)	Dep. I_H Dep. I_A (1)	Dep. I_H Hyp. I_A (4)	Hyp. I_H Dep. I_A (5)
I_H					
V_{50m}	−92.5	−96.9	−88.2	−85	−100
V_τ	−87.1	−91.9	−83.3	−80.1	−95.1
I_A					
V_{50m}	−40	−47.5	−32.5	−44.3	−35.7
V_{50h}	−73	−80.5	−65.5	−77.3	−68.7

Numbers in parentheses correspond to the combinations represented in Fig. 10*C*. All values are in mV. Hyp., Hyperpolarized; Dep., depolarized.

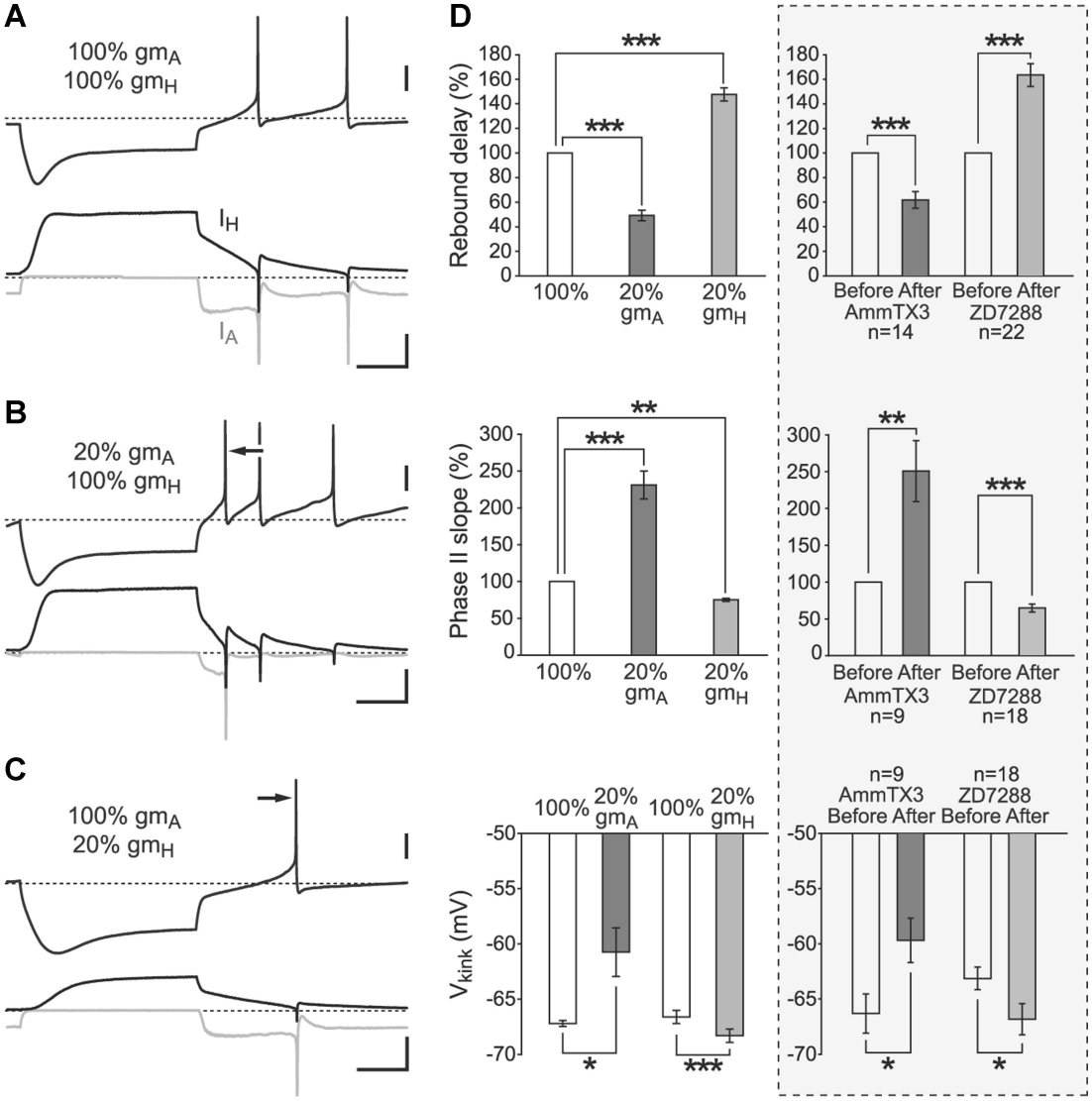

Figure 8. Dynamic clamp reproduces the effects of partial inhibition of I_A and I_H. ***A***, Rebound profile (top, black trace) of a neuron in response to the injection of average I_A (100% gm_A, bottom, light gray trace) and I_H (100% gm_H, bottom, black trace) conductances. ***B***, Rebound profile in the same neuron (top, black trace) with 20% gm_A and 100% gm_H. ***C***, Rebound profile in the same neuron (top, black trace) with 20% gm_H and 100% gm_A. ***D***, Left column, Bar plots summarizing the effects of reducing gm_A (20% gm_A) or gm_H (20% gm_H) on rebound delay, phase II slope, and V_{kink}. Right column (shaded box), Bar plots summarizing the effect of blocking 60 – 85% of the I_A and I_H currents with AmmTX3 and ZD7288, respectively, on the different rebound parameters. The bar plots showing the effect of AmmTX3 and ZD7288 on rebound delay were also presented in Figure 3*A*. Dashed lines indicate −60 mV (current-clamp) or 0 pA (dynamic clamp). $^*p < 0.05$, $^{**}p < 0.01$, $^{***}p < 0.001$.

To validate the dynamic-clamp system, we simulated the AmmTX3 and ZD7288 pharmacology experiments by reducing the injected conductances (gm_A or gm_H) to 20% of their original values (Fig. 8*A–D*). Reducing gm_A or gm_H qualitatively and quantitatively reproduced the effects of partial inhibition of I_A and I_H on all rebound parameters (Fig. 8*D*): reducing gm_A significantly decreased rebound delay ($p < 0.001$, $n = 5$, paired t test), increased phase II slope ($p = 0.002$, $n = 5$, paired t test), and depolarized V_{kink} ($p = 0.045$, $n = 5$, paired t test), while reducing gm_H significantly increased rebound delay ($p < 0.001$, $n = 5$, paired t test), decreased phase II slope ($p < 0.001$, $n = 5$), and hyperpolarized V_{kink} ($p < 0.001$, $n = 5$; Fig. 8*D*). It is especially striking that the dynamic clamp not only qualitatively reproduces the effects of AmmTX3 and ZD7288 on rebound parameters but also produces quantitative effects extremely similar to the effects of the toxins (Fig. 8*D*, left and right columns).

Covarying the amplitudes or the voltage dependences of I_H and I_A induces opposite effects on rebound delay

The covariation in amplitude of I_A and I_H has been proposed to represent a homeostatic mechanism (MacLean et al., 2003, 2005; Cao and Oertel, 2011). Our pharmacology experiments and their dynamic-clamp replicates indeed demonstrate that these two currents have opposite and complementary effects on rebound properties in dopaminergic neurons (Figs. 3, 8), suggesting that the covariation of their amplitudes should stabilize rebound properties. To demonstrate and quantify this principle, we simulated various combinations of gm_A and gm_H and analyzed the variations in rebound delays associated with these different sets of parameters (Fig. 9). We found that while different ratios of gm_A/gm_H yielded different values of rebound delay, modifying gm_A and gm_H while keeping the ratio constant (independent of its original value) tended to maintain the rebound delay value (Fig.

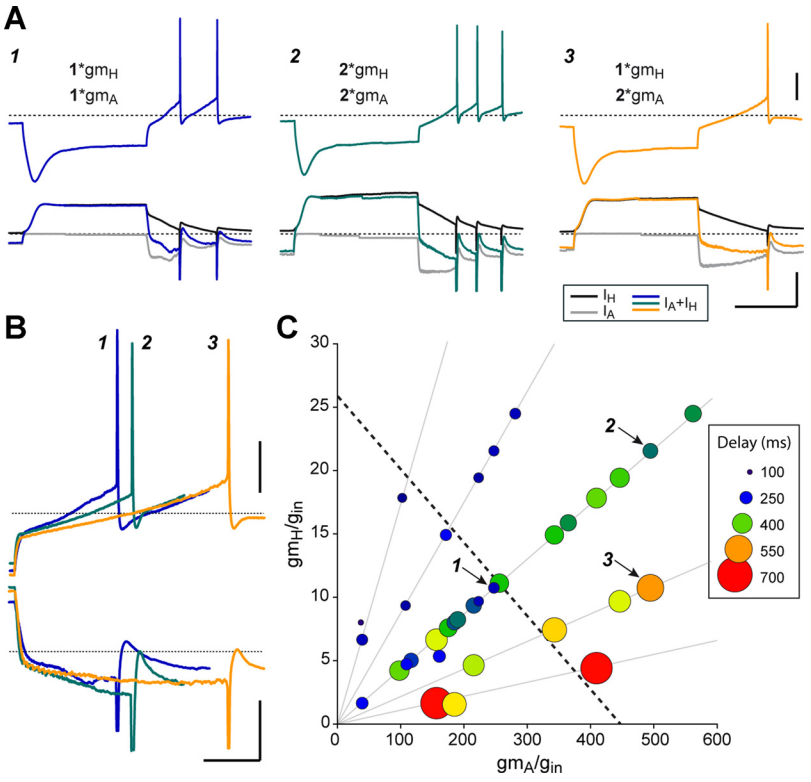

Figure 9. Effects of varying gm_A and gm_H on rebound delay. ***A***, Example traces showing the rebound profile (top traces) of the same neuron in response to the dynamic-clamp injection (I_H, bottom black trace; I_A, bottom gray trace; total injected current, bottom color trace) of various combinations of gm_H and gm_A: (1) 1 * gm_H, 1 * gm_A, (2) 2 * gm_H, 2 * gm_A, and (3) 1 * gm_H, 2 * gm_A with gm_H = 16.6 nS and gm_A = 380 nS. The numbers are used to identify the corresponding traces and points in ***B*** and ***C***. ***B***, Expanded superimposed current-clamp (top) and dynamic-clamp (bottom) traces corresponding to the traces shown in ***A***. ***C***, Summary bubble plot showing the effect of varying gm_A and gm_H on rebound delay. Increasing delay is coded by both color and size of the bubble: small blue bubbles correspond to short delays while big red bubbles correspond to long delays. Gray lines indicate constant ratio directions in parameter space. The dashed line corresponds to the direction of best sensitivity of delay in parameter space calculated by multiple linear regression of delay versus gm_A and gm_H (delay = 270 + 8.4 * gm_A − 146 * gm_H). In this plot, gm_A and gm_H were normalized to the input conductance of the neuron and do not have dimensions. Dashed lines indicate −60 mV (current-clamp) or 0 pA (dynamic clamp). Calibration: ***A***, Top, 20 mV; *A*, Bottom, 200 pA 500 ms; ***B***, Top, 20 mV; *B*, Bottom, 200 pA, 150 ms.

9*C*, gray lines). For example, modifying only gm_A while keeping gm_H constant induced a more pronounced change in delay than if both conductances were scaled together (Fig. 9*A*,*B*, traces 1–3). From these experiments, we were also able to determine the direction of maximum sensitivity of rebound delay in the parameter space (the optimal coordinated changes in gm_A and gm_H yielding maximal changes in delay): decreasing gm_H by approximately threefold while increasing gm_A by approximately fourfold (Fig. 9*C*, dotted line). Therefore, maintaining a constant ratio between I_A and I_H maximum conductances had a stabilizing (or homeostatic) effect on rebound properties.

To determine what functional impact the covariation of voltage dependences observed in our voltage-clamp experiments (Fig. 4*D*) might have, we also tested different combinations of I_A and I_H V_{50} values inside or outside the biological distribution of values while using average values for gm_A and gm_H (Table 2) and keeping them constant (Fig. 10). Only I_H activation V_{50} and I_A inactivation V_{50} are represented, but I_A activation V_{50} was also modified accordingly since it was found to be significantly correlated with I_H activation V_{50} and I_A inactivation V_{50} in voltage-clamp recordings. We specifically tested three combinations of values along the biological distribution centered on the mean of IA and IH V_{50} values (−73 ± 7.5 mV, −92.5 ± 4.35 mv, respectively; Fig. 10, conditions 1, 2, and 3), and compared these to a set of combinations equidistant and orthogonal to the biological distribution (Fig. 10, conditions 4 and 5). Interestingly, we found that the "biological" combinations of values were associated with a large variation in rebound delay (condition 1 vs 2, $p = 0.013$, $n = 5$; condition 3 vs 2, $p = 0.028$, $n = 5$, paired t test; Fig. 10) while "nonbiological" orthogonal combinations were associated with no significant change in rebound delay (condition 4 vs 2, $p = 0.256$, $n = 5$; condition 5 vs 2, $p = 0.84$, paired t test; Fig. 10). When using "biological" combinations, the changes in rebound delay were associated with changes in V_{kink} and phase II slope (Fig. 10*B*, example traces) consistent with the correlations observed in our voltage-clamp recordings (Fig. 6): hyperpolarizing the V_{50} values of I_A and I_H induced a significant hyperpolarization of the V_{kink} (average of −72.4 vs −66.9 mV, $p < 0.001$, $n = 5$, paired t test) and a decrease in phase II slope (45.9 vs 65.7 mV/s, $p = 0.002$, $n = 5$, paired t test), while depolarizing the V_{50} values had opposite and significant effects on V_{kink} (−61.2 vs −66.9 mV, $p < 0.001$, $n = 5$, paired t test) and phase II slope (82.8 vs 65.7 mV/s, $p < 0.001$, $n = 5$, paired t test). In contrast, for the orthogonal distribution, only the combination of depolarized I_A and hyperpolarized I_H (Fig. 10, condition 5) was associated with a slight depolarizing shift of V_{kink} (−65 vs −66.9 mV, $p = 0.03$, $n = 5$, paired t test). All other values were not significantly different from those obtained with the mean combination. Although the voltage dependences of other currents may covary with I_A and I_H V_{50} values in the biological population, these experiments demonstrate that the isolated covariation of I_A and I_H voltage dependences (while all other endogenous currents are not modified) is sufficient to accurately reproduce the correlations observed between the properties of I_A and I_H and the rebound profile in the biological population (Fig. 6). Thus, I_A and I_H properties have a critical influence on the response to inhibitory stimuli, independent of the variations in properties of other voltage-dependent currents.

Unlike the covariation of maximum conductances, the covariation of voltage dependences seems to essentially have a "nonhomeostatic" effect on rebound properties as it enhances the dynamic range of rebound values. Moreover, Figure 11 clearly shows that covarying the voltage dependences of I_A and I_H along the biological distribution (>15 mV and 8.7 mV, respectively) induced a similar change in rebound delay as changing gm_A/gm_H by fourfold, suggesting that covarying the voltage dependences of I_A and I_H constitutes a much more efficient way of tuning rebound delay.

Discussion

In the present study, we show that I_A and I_H voltage dependences are highly variable from cell to cell but strongly correlated in SNc dopaminergic neurons, and that this covariation is sensitive to

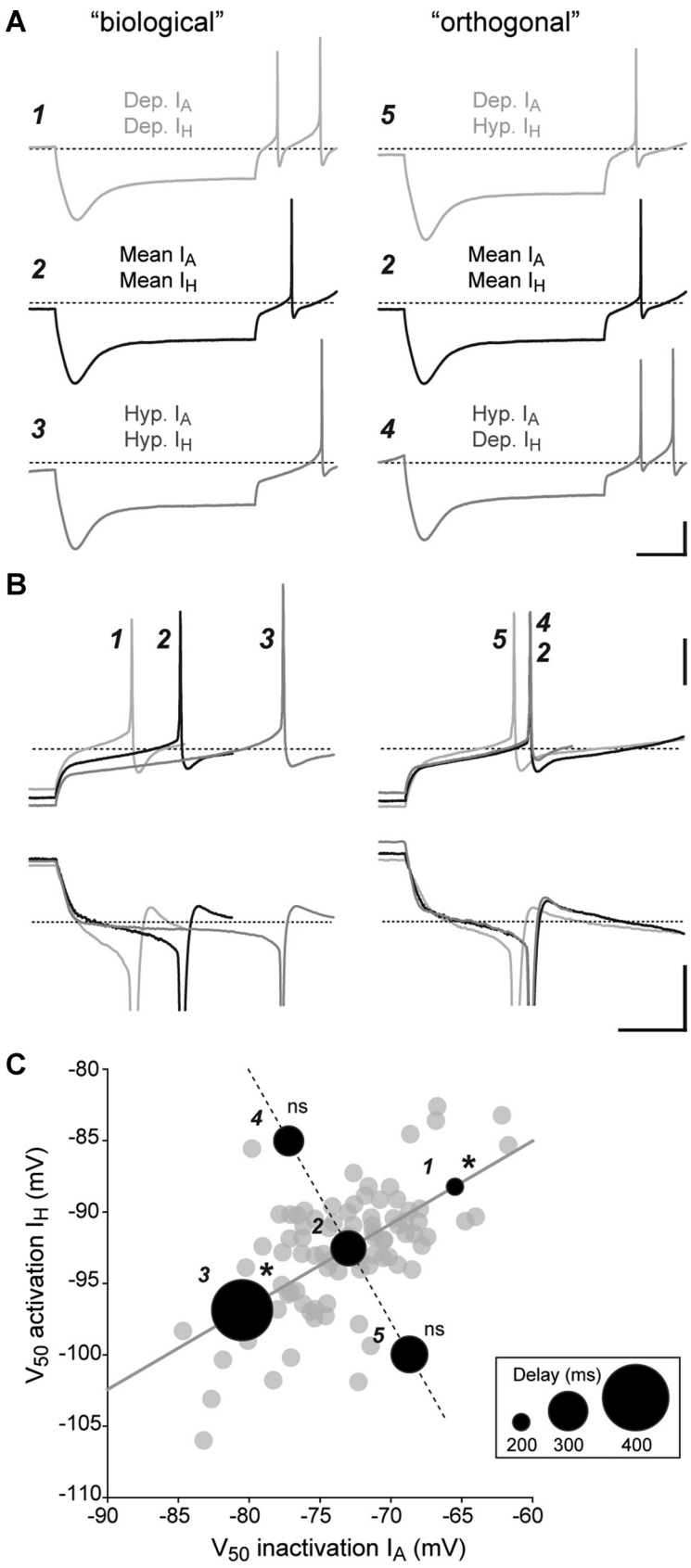

Figure 10. Effects of covarying I_H and I_A voltage dependences on rebound delay. ***A***, Left, Example current-clamp traces showing the rebound profile in the same neuron in response to the dynamic-clamp injection of "biological" combinations of voltage dependences of I_A and I_H (traces 1–3 correspond to depolarized, average biological values, and hyperpolarized V_{50} values, respectively; see *C*, corresponding points). Right, Example current-clamp traces showing the rebound profile in the same neuron in response to the dynamic-clamp injection of nonbiological "orthogonal" combinations of voltage dependences of I_A and I_H (traces 5, 2, and 4 correspond to hyperpolarized I_H V_{50} and depolarized I_A V_{50}, average biological V_{50} values, and depolarized I_H V_{50} and hyperpolarized I_A V_{50} respectively; see corresponding points in ***C***). ***B***, Expanded current-clamp (top) and dynamic-clamp (bottom) traces corresponding to the traces presented in ***A***. ***C***, Summary bubble plot showing the effect of varying I_A and I_H voltage dependences on rebound delay. Variations in delay are coded by the size of the black bubbles. Filled light-gray circles correspond to the biological distribution of V_{50} values (Fig. 4*D*) and the gray line indicates the linear regression of these values. The dashed line corresponds to the direction orthogonal to the biological distribution. Numbers correspond to the traces presented in ***A*** and ***B***. Asterisks indicate significant differences in delay compared with the mean value (2). ns, Nonsignificant. Calibration: ***A***, 20 mV, 250 ms; ***B***, Top, 20 mV; Bottom, 200 pA, 100 ms. Dashed lines indicate −60 mV (current-clamp) or 0 pA (dynamic clamp).

calcium and cAMP levels. Furthermore, we demonstrate that this covariation plays a critical role in tuning rebound delay as it confers synergistic functional effects to otherwise antagonistic currents. This is the first time that the covariation of voltage dependences of two distinct currents has been demonstrated, that signals involved in the covariation have been identified, and that the functional influence of this covariation on firing has been quantified.

Variability and covariation of biophysical properties of I_A and I_H in SNc dopaminergic neurons

Variability in the properties of ion channels is a physiological phenomenon observed in numerous systems (Liss et al., 2001; Golowasch et al., 2002; Neuhoff et al., 2002; MacLean et al., 2005; Swensen and Bean, 2005; Schulz et al., 2006, 2007; Khorkova and Golowasch, 2007; Goaillard et al., 2009; Temporal et al., 2011). So far, a threefold to fourfold range of variability has been reported mainly at the level of ion channel expression or current amplitude. We describe a high degree of variability in the amplitudes and voltage dependences of I_A and I_H and a significant covariation of their voltage dependences (Fig. 4). Studies have reported similar levels of variability in the amplitude of I_A (Liss et al., 2001) and I_H (Neuhoff et al., 2002) in mouse SNc dopaminergic neurons. Furthermore, consistent with invertebrate studies (Schulz et al., 2006), Liss et al. (2001) found that the amplitude of the I_A current scaled linearly with the level of expression of the Kv4.3 channel that underlies it. Our data are also consistent with previous reports of variability in the amplitude of I_H (measured at −120 mV) in SNc neurons associated with a high degree of variability in rebound delay: cells with a

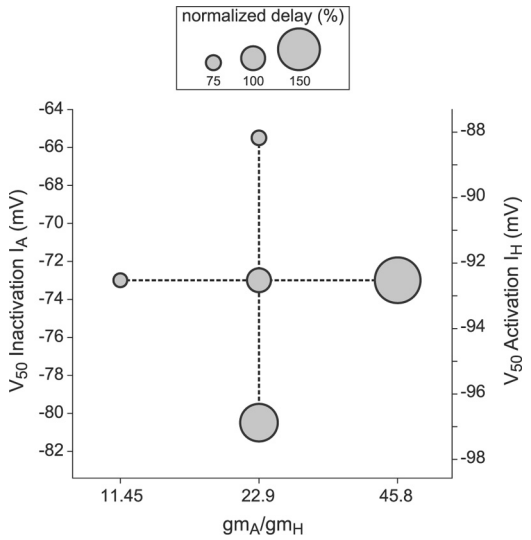

Figure 11. Comparing the effects of varying I_H and I_A voltage dependences or maximum conductances. Bubble plot showing the variations in normalized rebound delay (bubble diameter) associated with variable ratios of gm_A/gm_H (horizontally aligned bubbles) and the three different biological combinations of covarying voltage dependences of I_H and I_A (vertically aligned bubbles). Note that the changes in delay induced by a fourfold change in gm_A/gm_H and by a 15/8.7 mV shift in voltage dependences are of similar magnitude (small bubbles vs large bubbles).

large I_H (due to a depolarized activation voltage and/or high density of channels) tended to have faster rebounds (Neuhoff et al., 2002). Moreover, a recent study demonstrated that wortmannin [an inhibitor of phosphatidylinositol-4,5-bisphosphate (PIP2) synthesis] induced a negative shift in the voltage dependence of I_H associated with an increase in rebound delay in SNc dopaminergic neurons (Zolles et al., 2006).

Functional impact of the covariation on physiological activity patterns

Our dynamic-clamp experiments directly demonstrate that the covariation of the voltage dependences of I_A and I_H powerfully modifies rebound delay in SNc dopaminergic neurons (Fig. 10) and could play a critical role in shaping the response of these neurons to inhibitory inputs. Indeed, 70% of the synaptic inputs received by SNc dopaminergic neurons are GABAergic (Tepper and Lee, 2007), while dopamine release between neighboring cells is also responsible for long hyperpolarizations (Vandecasteele et al., 2008). A recent study using dynamic clamp in SNc dopaminergic neurons demonstrated that their response to trains of simulated GABAergic inputs was influenced by I_H properties (Tateno and Robinson, 2011). The partial inhibition of I_A and I_H (Figs. 3, 8) also clearly showed the involvement of these two currents in rebound responses to short (single simulated GABAergic-like event) or longer (1 s current step) hyperpolarizing stimuli, even for mild hyperpolarizations. I_A and I_H have also been reported to be involved in pacemaking activity in SNc neurons (Liss et al., 2001; Seutin et al., 2001; Neuhoff et al., 2002; Okamoto et al., 2006; Zolles et al., 2006; Chan et al., 2007; Puopolo et al., 2007; Guzman et al., 2009; Putzier et al., 2009; Tateno and Robinson, 2011). Although we did not investigate relationships between I_A and I_H and spontaneous activity, it is likely that the covariation of voltage dependences would also influence pacemaking activity. Studies have reported that changing I_H voltage dependence or amplitude induced significant changes in pacemaking frequency in SNc dopaminergic neurons (Zolles et al., 2006; Tateno and Robinson, 2011). Thus, the covariation of voltage dependences may also be relevant to understanding the regulation of SNc dopaminergic neuron firing in general.

Several studies indicate that the SNc dopaminergic neurons are heterogeneous, and that the intrinsic properties of these neurons may depend on (1) the localization of the neurons within the SNc or on their projection sites (Lammel et al., 2008; Liss and Roeper, 2008) or (2) the expression of the calcium-binding protein calbindin (Neuhoff et al., 2002). We found no relationship between I_A and I_H voltage dependences and the localization of the neurons in the SNc (for both mediolateral and rostrocaudal axes, $n = 47$ and 33, respectively; data not shown). Nonetheless, part of the variability in I_H, I_A, and rebound firing properties may be associated with the functional diversity of dopaminergic SNc neurons (Neuhoff et al., 2002; Lammel et al., 2008; Liss and Roeper, 2008).

Mechanisms underlying the covariation of voltage dependences

Our results demonstrate that calcium and cAMP potently modify the covariation of I_A and I_H voltage dependences (Fig. 6). The effects of BAPTA on I_A and 8-Br-cAMP on I_H are consistent with the well documented sensitivity of these currents to calcium and cAMP, respectively (Birnbaum et al., 2004; Sergeant et al., 2005; Zolles et al., 2006; Biel et al., 2009; Anderson et al., 2010). In addition, our data demonstrated a milder converse sensitivity of I_H and I_A to calcium and cAMP manipulation, respectively (Fig. 5). These data are consistent with the results from Chan et al. (2007) demonstrating that two of the three adenylyl cyclases expressed in SNc dopaminergic neurons are calcium-inhibited. Thus, the depolarization of I_H V_{50} values by BAPTA is probably due to the release of the calcium inhibition on the adenylyl cyclases and subsequent increase in cAMP. Conversely, little evidence is available regarding Kv4 modulation by the cAMP signaling pathway (Hoffman and Johnston, 1998; Yang et al., 2001; Lin et al., 2010). Hoffman and Johnston (1998) demonstrated that I_A inactivation and activation curves in hippocampal pyramidal neurons are depolarized by the cAMP-mediated activation of protein kinase A. Although pyramidal cells express only Kv4.2 (Chen et al., 2006), the high level of homology between Kv4.2 and Kv4.3 (including several phosphorylation sites) strongly suggests that Kv4.3 shares cAMP sensitivity (Schrader et al., 2002). Another study performed on SNc dopaminergic neurons also suggested that I_A amplitude is modulated by cAMP through MAPK activation (Yang et al., 2001). Finally, the application of BAPTA plus 8-Br-cAMP not only shifted I_A and I_H voltage dependences in a coordinated manner, but also dramatically reduced their variability (Fig. 5*C*). Altogether, these data suggest that the covariation of I_A and I_H voltage dependences is strongly dependent on calcium and cAMP. However, we do not conclude that these are the only signals involved in the covariation in voltage dependences. For example, as both HCN and Kv4 channels have been shown to be sensitive to PIP2, this signaling pathway may also be involved (Oliver et al., 2004; Zolles et al., 2006).

Although our experiments were performed using globally imposed changes in calcium and cAMP, these signals are most likely confined to submembrane microcompartments in physiological conditions. As the fast calcium chelator BAPTA (producing local calcium buffering), but not EGTA, was able to significantly reduce the variability in I_A and I_H V_{50} values (Fig. 5), local calcium variations are likely involved in the covariation of I_A/I_H. Consistent with these results, Anderson et al. (2010) demonstrated that

the Ca_v3-mediated modulation of I_A inactivation properties in cerebellar granule cells was also blocked by 10 mM BAPTA but not by 10 mM EGTA. Subsequently, they showed that the Ca_v3 calcium channel modulation of I_A relied on the formation of protein complexes comprising Kv4.2, KChip3.1, and Ca_v3 (Anderson et al., 2010). A similar molecular organization might be involved in the covariation of I_A and I_H voltage dependences in SNc dopaminergic neurons.

Coregulating conductances versus voltage dependences: homeostasis versus signal tuning?

Our dynamic-clamp results and other studies (MacLean et al., 2003; Cao and Oertel, 2011) demonstrate that I_H and I_A compensate each other and that firing properties are conserved when a constant gm_A/gm_H ratio between the two currents is maintained (Fig. 9). Therefore, the frequent correlation in the levels of mRNA for the channels carrying I_H and I_A (or in the current amplitude) in crustaceans (MacLean et al., 2005; Khorkova and Golowasch, 2007; Schulz et al., 2007; Tobin et al., 2009; Temporal et al., 2011) can be interpreted as a homeostatic mechanism. We demonstrated that a stable gm_A/gm_H ratio in SNc dopaminergic neurons indeed maintained rebound properties (Fig. 9) while the covariation in voltage dependences maximized the dynamic range of rebound delays (Fig. 10). Furthermore, our results show that covarying voltage dependences within the biological range of values has the same effect on rebound delay as changing the ratio between I_H and I_A maximum conductances by a factor of four (Fig. 11). This is especially striking since the range of values of V_{50} values used for the dynamic-clamp experiments covered only two-thirds of the total range observed in the voltage-clamp experiments. These values are also within the range of amplitudes of modulator-induced shifts in voltage dependence previously reported for I_A (Harris-Warrick et al., 1995; Yu et al., 1999; Birnbaum et al., 2004; Levy et al., 2010) or I_H (Harris-Warrick et al., 1995; Zolles et al., 2006; Biel et al., 2009). Data obtained in SNc dopaminergic neurons (Liss et al., 2001) and in invertebrates (MacLean et al., 2003; Schulz et al., 2006, 2007; Tobin et al., 2009; Temporal et al., 2011) suggest that changing the ratio of maximum conductances may rely on changing the levels of expression of the underlying channels. Alternatively, it could involve internalization of channels and/or degradation of channel proteins or mRNAs. However, such processes would be energy expensive and occur on a minute-to-hour time scale. Covarying voltage dependences represents a highly computationally efficient and energy-efficient way of tuning rebound properties. As the covariation of voltage dependences of I_A and I_H involves small signaling molecules (including calcium and cAMP) that can exhibit rapid dynamics, this covariation also provides a highly flexible way of tuning rebound properties. Therefore, in any given neuronal type, the appropriate firing pattern may be approximately achieved (coarse tuning) by coregulation of the expression of functionally overlapping ion channels (such as Kv4.3 and HCN in SNc dopaminergic neurons), with the coregulation of gating properties allowing for a secondary flexible fine-tuning of firing. Whether this tuning would occur in response to acute external signals, such as neurotransmitters or neuromodulators, or in response to chronic changes in excitability, is yet to be determined.

References

An WF, Bowlby MR, Betty M, Cao J, Ling HP, Mendoza G, Hinson JW, Mattsson KI, Strassle BW, Trimmer JS, Rhodes KJ (2000) Modulation of A-type potassium channels by a family of calcium sensors. Nature 403:553–556.

Anderson D, Mehaffey WH, Iftinca M, Rehak R, Engbers JD, Hameed S, Zamponi GW, Turner RW (2010) Regulation of neuronal activity by Cav3-Kv4 channel signaling complexes. Nat Neurosci 13:333–337.

Biel M, Wahl-Schott C, Michalakis S, Zong X (2009) Hyperpolarization-activated cation channels: from genes to function. Physiol Rev 89:847–885.

Birnbaum SG, Varga AW, Yuan LL, Anderson AE, Sweatt JD, Schrader LA (2004) Structure and function of Kv4-family transient potassium channels. Physiol Rev 84:803–833.

Burdakov D (2005) Gain control by concerted change in I_A and I_H conductances. Neural Comput 17:991–995.

Cao XJ, Oertel D (2011) The magnitudes of hyperpolarization-activated and low-voltage-activated potassium currents covary in neurons of the ventral cochlear nucleus. J Neurophysiol 106:630–640.

Chan CS, Guzman JN, Ilijic E, Mercer JN, Rick C, Tkatch T, Meredith GE, Surmeier DJ (2007) 'Rejuvenation' protects neurons in mouse models of Parkinson's disease. Nature 447:1081–1086.

Chen X, Yuan LL, Zhao C, Birnbaum SG, Frick A, Jung WE, Schwarz TL, Sweatt JD, Johnston D (2006) Deletion of *Kv4.2* gene eliminates dendritic A-type K^+ current and enhances induction of long-term potentiation in hippocampal CA1 pyramidal neurons. J Neurosci 26:12143–12151.

Franz O, Liss B, Neu A, Roeper J (2000) Single-cell mRNA expression of HCN1 correlates with a fast gating phenotype of hyperpolarization-activated cyclic nucleotide-gated ion channels (Ih) in central neurons. Eur J Neurosci 12:2685–2693.

Goaillard JM, Taylor AL, Schulz DJ, Marder E (2009) Functional consequences of animal-to-animal variation in circuit parameters. Nat Neurosci 12:1424–1430.

Goldman MS, Golowasch J, Marder E, Abbott LF (2001) Global structure, robustness, and modulation of neuronal models. J Neurosci 21:5229–5238.

Golowasch J, Goldman MS, Abbott LF, Marder E (2002) Failure of averaging in the construction of a conductance-based neuron model. J Neurophysiol 87:1129–1131.

Grace AA, Onn SP (1989) Morphology and electrophysiological properties of immunocytochemically identified rat dopamine neurons recorded *in vitro*. J Neurosci 9:3463–3481.

Guzman JN, Sánchez-Padilla J, Chan CS, Surmeier DJ (2009) Robust pacemaking in substantia nigra dopaminergic neurons. J Neurosci 29:11011–11019.

Hahn J, Tse TE, Levitan ES (2003) Long-term K^+ channel-mediated dampening of dopamine neuron excitability by the antipsychotic drug haloperidol. J Neurosci 23:10859–10866.

Harris-Warrick RM, Coniglio LM, Levini RM, Gueron S, Guckenheimer J (1995) Dopamine modulation of two subthreshold currents produces phase shifts in activity of an identified motoneuron. J Neurophysiol 74:1404–1420.

Hille B (2001) Ion channels of excitable membranes, Ed 3. Sunderland, MA: Sinauer.

Hoffman DA, Johnston D (1998) Downregulation of transient K^+ channels in dendrites of hippocampal CA1 pyramidal neurons by activation of PKA and PKC. J Neurosci 18:3521–3528.

Hudson AE, Prinz AA (2010) Conductance ratios and cellular identity. PLos Comput Biol 6:e1000838.

Khorkova O, Golowasch J (2007) Neuromodulators, not activity, control coordinated expression of ionic currents. J Neurosci 27:8709–8718.

Kita T, Kita H, Kitai ST (1986) Electrical membrane properties of rat substantia nigra compacta neurons in an in vitro slice preparation. Brain Res 372:21–30.

Kitai ST, Shepard PD, Callaway JC, Scroggs R (1999) Afferent modulation of dopamine neuron firing patterns. Curr Opin Neurobiol 9:690–697.

Lammel S, Hetzel A, Häckel O, Jones I, Liss B, Roeper J (2008) Unique properties of mesoprefrontal neurons within a dual mesocorticolimbic dopamine system. Neuron 57:760–773.

Levy DI, Cepaitis E, Wanderling S, Toth PT, Archer SL, Goldstein SA (2010) The membrane protein MiRP3 regulates Kv4.2 channels in a KChIP-dependent manner. J Physiol 588:2657–2668.

Lin L, Sun W, Wikenheiser AM, Kung F, Hoffman DA (2010) KChIP4a regulates Kv4.2 channel trafficking through PKA phosphorylation. Mol Cell Neurosci 43:315–325.

Liss B, Roeper J (2008) Individual dopamine midbrain neurons: functional diversity and flexibility in health and disease. Brain Res Rev 58:314–321.

Liss B, Franz O, Sewing S, Bruns R, Neuhoff H, Roeper J (2001) Tuning pacemaker frequency of individual dopaminergic neurons by Kv4.3L and KChip3.1 transcription. EMBO J 20:5715–5724.

MacLean JN, Zhang Y, Johnson BR, Harris-Warrick RM (2003) Activity-independent homeostasis in rhythmically active neurons. Neuron 37:109–120.

MacLean JN, Zhang Y, Goeritz ML, Casey R, Oliva R, Guckenheimer J, Harris-Warrick RM (2005) Activity-independent coregulation of IA and Ih in rhythmically active neurons. J Neurophysiol 94:3601–3617.

Marder E, Goaillard JM (2006) Variability, compensation and homeostasis in neuron and network function. Nat Rev Neurosci 7:563–574.

Marder E, Taylor AL (2011) Multiple models to capture the variability in biological neurons and networks. Nat Neurosci 14:133–138.

Nedergaard S (1999) Regulation of action potential size and excitability in substantia nigra compacta neurons: sensitivity to 4-aminopyridine. J Neurophysiol 82:2903–2913.

Neuhoff H, Neu A, Liss B, Roeper J (2002) I_h channels contribute to the different functional properties of identified dopaminergic subpopulations in the midbrain. J Neurosci 22:1290–1302.

Okamoto T, Harnett MT, Morikawa H (2006) Hyperpolarization-activated cation current (Ih) is an ethanol target in midbrain dopamine neurons of mice. J Neurophysiol 95:619–626.

Oliver D, Lien CC, Soom M, Baukrowitz T, Jonas P, Fakler B (2004) Functional conversion between A-type and delayed rectifier K+ channels by membrane lipids. Science 304:265–270.

Patel SP, Campbell DL, Strauss HC (2002) Elucidating KChIP effects on Kv4.3 inactivation and recovery kinetics with a minimal KChIP2 isoform. J Physiol 545:5–11.

Prinz AA, Bucher D, Marder E (2004) Similar network activity from disparate circuit parameters. Nat Neurosci 7:1345–1352.

Puopolo M, Raviola E, Bean BP (2007) Roles of subthreshold calcium current and sodium current in spontaneous firing of mouse midbrain dopamine neurons. J Neurosci 27:645–656.

Putzier I, Kullmann PH, Horn JP, Levitan ES (2009) Dopamine neuron responses depend exponentially on pacemaker interval. J Neurophysiol 101:926–933.

Robinson HP (2008) A scriptable DSP-based system for dynamic conductance injection. J Neurosci Methods 169:271–281.

Schrader LA, Anderson AE, Mayne A, Pfaffinger PJ, Sweatt JD (2002) PKA modulation of Kv4.2-encoded A-type potassium channels requires formation of a supramolecular complex. J Neurosci 22:10123–10133.

Schulz DJ, Goaillard JM, Marder E (2006) Variable channel expression in identified single and electrically coupled neurons in different animals. Nat Neurosci 9:356–362.

Schulz DJ, Goaillard JM, Marder EE (2007) Quantitative expression profiling of identified neurons reveals cell-specific constraints on highly variable levels of gene expression. Proc Natl Acad Sci U S A 104:13187–13191.

Sergeant GP, Ohya S, Reihill JA, Perrino BA, Amberg GC, Imaizumi Y, Horowitz B, Sanders KM, Koh SD (2005) Regulation of Kv4.3 currents by Ca2+/calmodulin-dependent protein kinase II. Am J Physiol Cell Physiol 288:C304–C313.

Seutin V, Massotte L, Renette MF, Dresse A (2001) Evidence for a modulatory role of Ih on the firing of a subgroup of midbrain dopamine neurons. Neuroreport 12:255–258.

Storm JF, Vervaeke K, Hu H, Graham LJ (2009) Functions of the persistent Na+ current in cortical neurons revealed by dynamic clamp. In: Dynamic-clamp: from principles to applications (Destexhe A, Bal T, eds), pp 165–197. New York: Springer.

Swensen AM, Bean BP (2005) Robustness of burst firing in dissociated Purkinje neurons with acute or long-term reductions in sodium conductance. J Neurosci 25:3509–3520.

Tanaka Y, Furuyashiki T, Momiyama T, Namba H, Mizoguchi A, Mitsumori T, Kayahara T, Shichi H, Kimura K, Matsuoka T, Nawa H, Narumiya S (2009) Prostaglandin E receptor EP1 enhances GABA-mediated inhibition of dopaminergic neurons in the substantia nigra pars compacta and regulates dopamine level in the dorsal striatum. Eur J Neurosci 30:2338–2346.

Tateno T, Robinson HP (2011) The mechanism of ethanol action on midbrain dopaminergic neuron firing: a dynamic-clamp study of the role of Ih and GABAergic synaptic integration. J Neurophysiol 106:1901–1922.

Taylor AL, Goaillard JM, Marder E (2009) How multiple conductances determine electrophysiological properties in a multicompartment model. J Neurosci 29:5573–5586.

Temporal S, Desai M, Khorkova O, Varghese G, Dai A, Schulz DJ, Golowasch J (2012) Neuromodulation independently determines correlated channel expression and conductance levels in motor neurons of the stomatogastric ganglion. J Neurophysiol. 21:3443–3456.

Tepper JM, Lee CR (2007) GABAergic control of substantia nigra dopaminergic neurons. Prog Brain Res 160:189–208.

Tobin AE, Cruz-Bermúdez ND, Marder E, Schulz DJ (2009) Correlations in ion channel mRNA in rhythmically active neurons. PLoS One 4:e6742.

Vacher H, Alami M, Crest M, Possani LD, Bougis PE, Martin-Eauclaire MF (2002) Expanding the scorpion toxin alpha-KTX 15 family with AmmTX3 from Androctonus mauretanicus. Eur J Biochem 269:6037–6041.

Vacher H, Prestipino G, Crest M, Martin-Eauclaire MF (2004) Definition of the alpha-KTx15 subfamily. Toxicon 43:887–894.

Vandecasteele M, Glowinski J, Deniau JM, Venance L (2008) Chemical transmission between dopaminergic neuron pairs. Proc Natl Acad Sci U S A 105:4904–4909.

Wolfart J, Neuhoff H, Franz O, Roeper J (2001) Differential expression of the small-conductance, calcium-activated potassium channel SK3 is critical for pacemaker control in dopaminergic midbrain neurons. J Neurosci 21:3443–3456.

Yang F, Feng L, Zheng F, Johnson SW, Du J, Shen L, Wu CP, Lu B (2001) GDNF acutely modulates excitability and A-type K+ channels in midbrain dopaminergic neurons. Nat Neurosci 4:1071–1078.

Yu H, McKinnon D, Dixon JE, Gao J, Wymore R, Cohen IS, Danilo P Jr, Shvilkin A, Anyukhovsky EP, Sosunov EA, Hara M, Rosen MR (1999) Transient outward current, Ito1, is altered in cardiac memory. Circulation 99:1898–1905.

Zolles G, Klöcker N, Wenzel D, Weisser-Thomas J, Fleischmann BK, Roeper J, Fakler B (2006) Pacemaking by HCN channels requires interaction with phosphoinositides. Neuron 52:1027–1036.